THE PREDICTION OF MILLIMETER WAVELENGTH PRECIPITATION ATTENUATION USING A CYLINDRICAL STORM CELL MODEL

L.R. Zintsmaster and D.B. Hodge

The Ohio State University

ElectroScience Laboratory

Department of Electrical Engineering
Columbus, Ohio 43212

TECHNICAL REPORT 2374-10

June 1972

Grant Number NGR 36-008-080

National Aeronautics and Space Administration
Office of Grants and Research Contracts
Washington, D.C. 20546

NOTICES

When Government drawings, specifications, or other data are used for any purpose other than in connection with a definitely related Government procurement operation, the United States Government thereby incurs no responsibility nor any obligation whatsoever, and the fact that the Government may have formulated, furnished, or in any way supplied the said drawings, specifications, or other data, is not to be regarded by implication or otherwise as in any manner licensing the holder or any other person or corporation, or conveying any rights or permission to manufacture, use, or sell any patented invention that may in any way be related thereto.

REPORT
by
THE OHIO STATE UNIVERSITY ELECTROSCIENCE LABORATORY
(FORMERLY ANTENNA LABORATORY)
Columbus, Ohio 43212

Sponsor	National Aeronautics and Space Administration Office of Grants and Research Contracts Washington, D.C. 20546
Grant Number	NGR 36-008-080
Investigation of	Millimeter-Wavelengths Propagation Studies
Subject of Report	THE PREDICTION OF MILLIMETER WAVELENGTH PRECIPITATION ATTENUATION USING A CYLINDRICAL STORM CELL MODEL
Authors	L.R. Zintsmaster and D.B. Hodge
Submitted by	L.R. Zintsmaster and D.B. Hodge ElectroScience Laboratory Department of Electrical Engineering The Ohio State University
Date	June 1972

FOREWORD

The material contained in this report is also used as a thesis submitted to the Department of Electrical Engineering, The Ohio State University as partial fulfillment of the requirements for the degree Master of Science.

ABSTRACT

The single terminal and two terminal diversity precipitation attenuation distributions are calculated for a millimeter wavelength earth-satellite propagation path. The calculated probability distributions are compared to attenuation probability distributions measured at two locations with the ATS-5 Millimeter Wavelength Experiment 15.63 GHz downlink. Using an empirically derived three mode exponential cell diameter - rain rate function, the calculated distributions agreed within -2 to +1 dB of the measured distributions for both terminal locations. The sensitivity of the calculated distribution to variations of the cell model parameters was also investigated.

TABLE OF CONTENTS

CHAPTER I
INTRODUCTION

The need for more satellite communications channels has recently stimulated interest in the millimeter wavelength portion of the spectrum. The approval of new channels above 10 GHz by the World Administrative Radio Conference[1] and the proposal of several domestic satellite communications systems[2] in 1971 indicate the extent of this interest. However, before such frequencies can be used efficiently, more information is needed about the propagation phenomena which occur at these wavelengths. It has been known for some time that atmospheric components can attenuate millimeter wavelength signals significantly, as shown in Fig. 1. The greatest attenuation is caused by high liquid precipitation rates occurring along the propagation path. However, there is little data available about the effects of precipitation which are useful to an engineer designing a millimeter wavelength earth-satellite communications link. To study these precipitation effects and develop propagation prediction techniques for system design, a millimeter wavelength experiment which included path attenuation measurements at 15.3 GHz and 31.65 GHz was included on-board the Applications Technology Satellite, ATS-5[3].

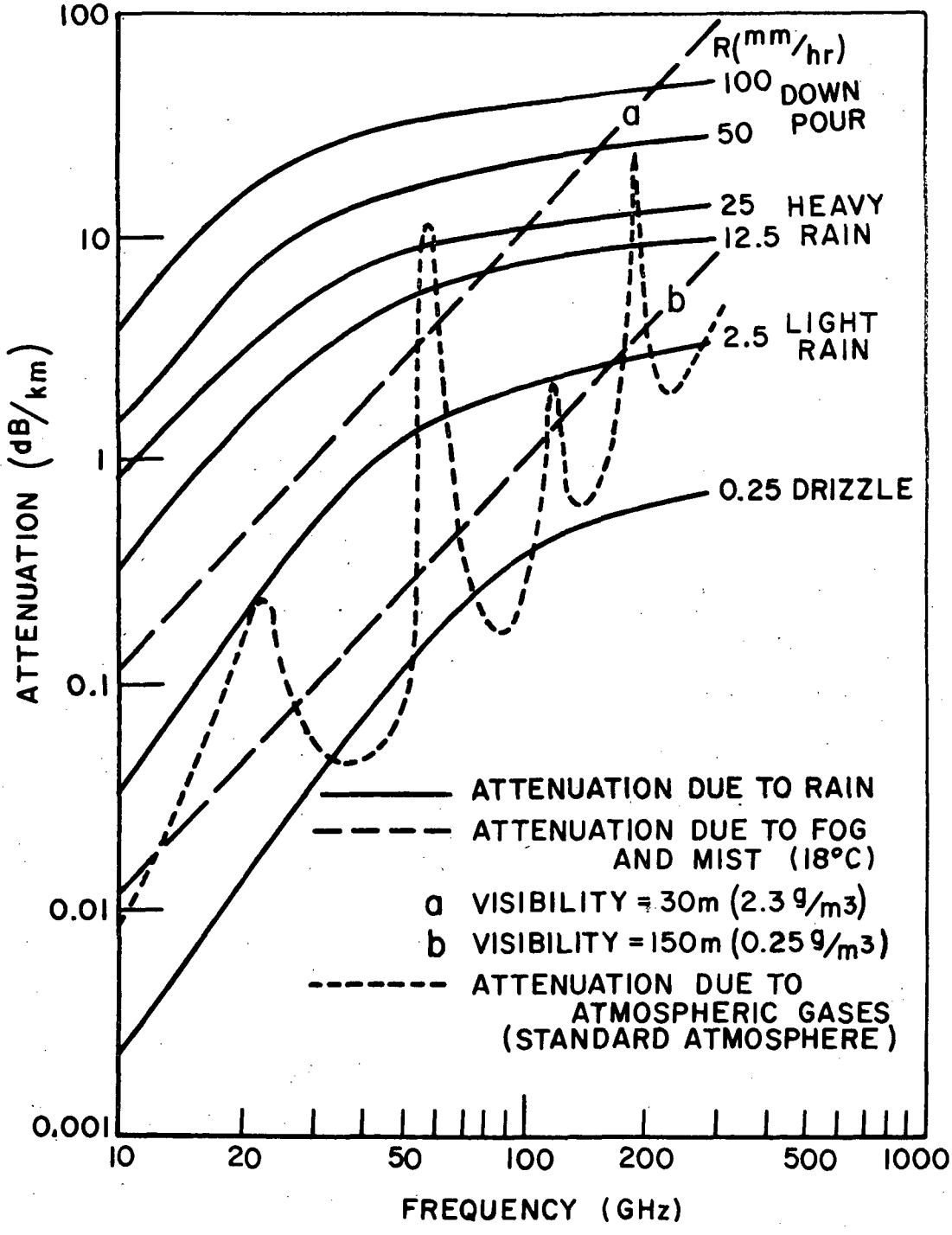

Fig. 1.--Attenuation due to gas absorption, fog and mist, and rain at millimeter wave frequencies (from Mondre[26]).

The attenuation probability distribution function is frequently used to predict long term effects of precipitation. This function gives the percentage of time that a particular level of attenuation is equalled or exceeded or, conversely, the system margin required to insure that the system is operational for a given percentage of time. Thus, it is useful in determining the economic feasibility and link reliability in system applications. This distribution function is strongly dependent upon the climatology of the region in which the earth terminal is located. Thus, the system designer needs a technique for predicting the precipitation attenuation probability distribution function for various earth terminal locations.

A simple, mathematically tractable storm cell model is used to make precipitation attenuation distribution predictions for a single earth terminal and a two-terminal diversity configuration. The calculated distributions are integrals of a rain rate probability density and an intersected path length probability distribution. The rain rate probability density is determined from tipping bucket rain gauge measurements. Thus, the statistical characteristics of precipitation events in different locations are included in the calculated attenuation distribution. A technique for using National Weather Service rain measurements is described so that easily available data can be used. The intersected path length probability distribution is calculated using a right circular cylinder with homogeneous rain rate, variable diameter and fixed height as a storm cell model. In this way, as a storm cell model, the physical characteristics of the precipitation events are represented.

Previous models used to estimate attenuation caused by rain have been based on postulating or measuring a precipitation distribution in a vertical slice along the propagation path. Dutton[4] assumed a spherical storm cell with a Gaussian variation of precipitation with altitude. The resulting attenuation calculated for a single fixed cell was an integral over the propagation path and a function of cell center location. This model is of limited use because it is difficult to incorporate the features which are needed to calculate the attenuation distribution. First, the statistical characteristics of the rain rate which must be added are hard to include. Second, the ways in which the cell might intersect the path to produce a particular attenuation are difficult to determine because of the vertical inhomogenity of the rain rate. Thus, a simpler model is required. A model proposed by Bradley[5] postulated a precipitation rate versus time model for an average storm in the geographic area of his interest. This model was then used to estimate the mean time between peak attenuation occurrences for a horizontal path. Although this approach uses the precipitation characteristics of a particular location, application is limited to horizontal paths.

The approach which is used here is to lump the effects of all liquid precipitation events together and model them with a single cylindrical storm cell. This model is described and the attenuation probability distribution function for a single terminal is calculated in Chapter II. In Chapter III, the model is extended to a two

terminal spatial diversity configuration and the joint attenuation probability distribution is calculated. The parameters which are used to relate the cell model to the physical world are discussed in Chapter IV. In Chapter V, calculated results are compared to propagation data measured by two terminals using the ATS-5 15.63 GHz downlink. The sensitivity of the model to parameter variations is also discussed and a diameter - rain rate function is proposed which improves the agreement of the calculated results.

CHAPTER II
CALCULATION OF THE SINGLE TERMINAL ATTENUATION PROBABILITY DISTRIBUTION

As described earlier, previous methods for predicting attenuation due to rain have all used some type of rainstorm model. But the models proposed could not be readily applied to solving the communications design problem because they were too specific and could not be used in other geographic regions. Another practical constraint which is imposed by the design problem is that the model should be mathematically tractable.

A reasonable approximation for the shape of a rainstorm is a cylinder. Thus, a right circular cylinder is used to model the precipitation phenomenon. To maintain the simplicity of the model, the precipitation in the cell is assumed to be in the form of rain only and the precipitation rate, r, is assumed to be non-zero and uniform throughout the cell. The cell diameter, denoted by d(r), is a function of the rain rate and represents an effective cell diameter. Consequently, the storm cell diameter may not compare well with observed rainstorm cell dimensions.

The origin of the coordinate system will coincide with the earth terminal location on a flat earth such that the terminal-satellite propagation path lies in the x-z plane. The elevation angle,

ξ, will be defined from the x-axis toward the z-axis. The proposed rainstorm model with the coordinate axes is shown in Fig. 2. The

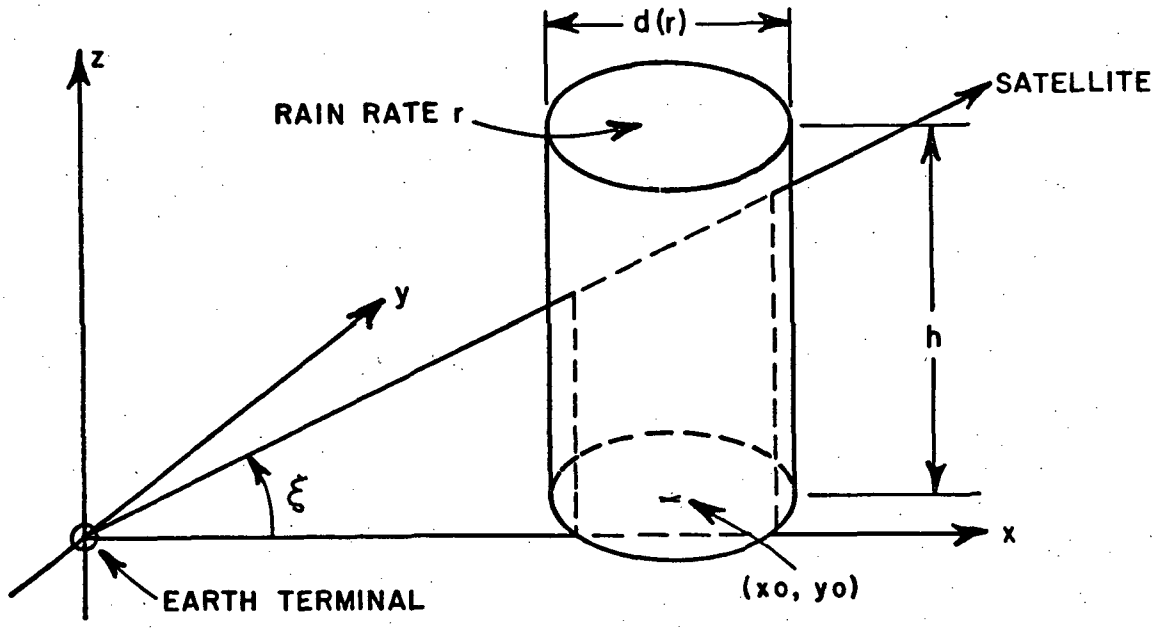

Fig. 2.--Earth terminal and storm cell model.

center of a storm cell will be defined as the point (x_0,y_0) where the vertical axis of the cell intersects the x-y plane. The occurrence of a storm cell centered at a point within the universe of storm cell centers is assumed to space-time ergodic. Thus, the time statistics of cell center occurrences observed at a point are equivalent to the spatial statistics of cell center occurrences at a particular point observed over the universe of cell center locations. The probability of a model cell centered at a point is assumed to be uniform over the universe of cell centers.

Before calculating the single terminal attenuation probability distribution function, the physical processes involved will be

considered to determine the variables whose probability functions are needed. For non-zero attenuation to occur along the propagation path a section of the propagation path must be intersected by the storm cell. The rain rate along this intersected section of the propagation path and the length of the intersected path, ℓ, determine the magnitude of the attenuation according to the Gunn-East equation[7]. The intersected path length can be calculated directly from the intersection geometry. Thus, to compute the attenuation probability distribution function, the storm cell rain rate probability density function and an intersected path length probability density function are needed.

Therefore, for the random variables r and ℓ, define

(1) $p_r(r)$ = probability density function of the rain rate r in a model storm cell

and

(2) $p_\ell(\ell)$ = probability density function of the length of the propagation path intersected by the storm cell.

Since $p_r(r)$ and $p_\ell(\ell)$ are probability density functions then

$$(3) \qquad \int_0^\infty p_r(r)\, dr = 1$$

and

$$\int_0^{\ell_{max}} p_\ell(\ell)\, d\ell = 1, \tag{4}$$

where ℓ_{max} is the maximum intersected path length.

The Gunn-East relation[7] mentioned previously gives a functional relation between the random variables, r and ℓ, and the attenuation, α, in dB,

$$\alpha = kr^p\ell. \tag{5}$$

The constants k and p are frequency and temperature dependent. Using a functional transformation theorem[8] for functions of two random variables it is found that for the two functions

$$\alpha = kr^p\ell \tag{6}$$

$$r = r \tag{7}$$

that

$$p_{\alpha,r}(\alpha,r) = p_{r,\ell}(r,\ell)/|J(r,\ell)| \tag{8}$$

where $p_{\alpha,r}(\alpha,r)$ is the joint probability density function of a rain rate r occurring on the intersected portion of the propagation path and the total attenuation occurring along the propagation path is α. The function $p_{r,\ell}(r,\ell)$ is the joint probability density function that a rain rate r occurs on the intersected path and the length of the

intersected propagation path on which the rain rate occurs is ℓ. Finally, $J(r,\ell)$ is the Jacobian of the functions α and r. The intersected path length, ℓ, shown in Eq. (8) is the solution of Eqs. (6) and (7) in terms of α and r,

$$\ell = \alpha/kr^p. \tag{9}$$

From an examination of the physical processes which are modelled by the storm cell it is clear that the occurrence of the rain rate, r, is independent of the occurrence of the intersected path length, ℓ. Thus,

$$p_{r,\ell}(r,\ell) = p_r(r)\, p_\ell(\ell). \tag{10}$$

The Jacobian in Eq. (8) is given by

$$J(r,\ell) = -kr^p. \tag{11}$$

Substituting Eqs. (9)-(11) into Eq. (8) the result is

$$p_{\alpha,r}(\alpha,r) = p_r(r)\, p_\ell(\alpha/kr^p)/kr^p. \tag{12}$$

If a storm cell having finite dimensions is considered, there is a maximum path intersection length, ℓ_{max}; and, consequently, for a given attenuation, α, there is a minimum rain rate, $r_{min}(\alpha)$, which is

$$r_{min}(\alpha) = (\alpha/k\ell_{max})^{1/p}. \tag{13}$$

Thus, the attenuation probability density function, $p_\alpha(\alpha)$, can be found from $p_{\alpha,r}(\alpha,r)$ by integrating r over the range $r_{min}(\alpha)$ to ∞ which yields

$$(14) \qquad p_\alpha(\alpha) = \int_{r_{min}(\alpha)}^{\infty} p_r(r)\, p_\ell(\alpha/kr^p)/kr^p \, dr.$$

The attenuation probability distribution function $P_\alpha(\alpha_o)$, which is defined as the probability that the attenuation, α_o, is equalled or exceeded is given in Eq. (15).

$$(15) \qquad P_\alpha(\alpha_o) = \int_{\alpha_o}^{\infty} p_\alpha(\alpha)\, d\alpha.$$

Substituting then $P_\alpha(\alpha_o)$ is

$$(16) \qquad P_\alpha(\alpha_o) = \int_{\alpha_o}^{\infty} \int_{r_{min}(\alpha)}^{\infty} p_r(r)\, p_\ell(\alpha/kr^p)/kr^p \, dr\, d\alpha.$$

To obtain an expression for $P_\alpha(\alpha_o)$ in terms of r and ℓ only let

$$(17a) \qquad x = r$$

$$(17b) \qquad y = kr^p\ell$$

$$(18a) \qquad u = r$$

$$(18b) \qquad v = \ell$$

and use Eq. (19) for transforming variables in a multiple integration

(19) $$\iint_R f(x,y)dxdy = \iint_{R'} f(x(u,v),y(u,v))|J(x,y)|dudv,$$

where $J(x,y)$ is the Jacobian, R is the region of the xy integration and R' is the corresponding region of the uv integration. Performing the indicated operations the result is

(20) $$P_\alpha(\alpha_o) = \int_{r_{min}(\alpha_o)}^{\infty} \int_{\ell_1(\alpha_o,r)}^{\ell_{max}} p_r(r)\, p_\ell(\ell)\, d\ell\, dr$$

with the new function $\ell_1(\alpha_o,r)$ defined as

(21) $\ell_1(\alpha_o,r)$ = minimum intersected path length needed to produce an attenuation α_o given the rain rate, r.

The function $\ell_1(\alpha_o,r)$ is a consequence of transforming the integration from the α,r plane to the r,ℓ plane and is given as

(22) $$\ell_1(\alpha_o,r) = \alpha_o/kr^p$$

and $r_{min}(\alpha_o)$ is given by

(23) $$r_{min}(\alpha_o) = (\alpha_o/k\ell_{max})^{1/p}.$$

The ℓ integration defines the probability distribution function, $P_\ell(\ell)$, which is the probability that the intersected path length equals or exceeds ℓ. Thus, the final form for $P_\alpha(\alpha_o)$ is

$$P_\alpha(\alpha_o) = N \int_{r_{min}(\alpha_o)}^{\infty} p_r(r)\, P_\ell(\ell_1(\alpha_o, r))\, dr, \tag{24}$$

where N is a normalization constant which is included to insure that $P_\alpha(o) = 1$. Thus, it is given by

$$N = 1/\int_{o}^{\infty} p_r(r)\, P_\ell(\ell_1(0, r))\, dr. \tag{25}$$

In order to use Eq. (24) for numeric calculations, two probability functions, $p_r(r)$ and $P_\ell(\ell)$, must be calculated. It is clear from the definition of $P_\ell(\ell)$ that it is calculated from the storm intersection geometry. The rain rate probability function $p_r(r)$, will be determined from meteorological measurements made in the geographical region of interest.

One way in which rain rate probability functions are measured is through the use of a tipping bucket rain gauge. Briefly, this gauge measures the time that it takes for a fixed amount of rain to fall. The number of tips occurring in a given time period then determine the average rain rate over that time period. The National Weather Service generally uses gauges which record a tip when 0.01 inch of rain falls and the number of tips occurring in a sixty minute period beginning on-the-hour are recorded and published[9]. Since these measurements are available for weather stations over the entire United States, the tipping bucket rain rate probability density function $p_B(r)$, which is defined as the probability density

of the rain rate r measured by a tipping bucket, will be used to calculate $p_r(r)$. In this way the geographic variation of precipitation phenomena is included in the attenuation probability calculation.

Before this is done, it should be observed that the sixty minute averaging time used in the National Weather Service measurements is too coarse for accurate estimations of $P_\alpha(\alpha_o)$. However, a method will be presented later which permits the estimation of a clock-minute rain rate probability density function from the clock-hourly rain rate probability distribution function. Although, it would be best to have the instantaneous rain rate probability density function, currently the clock-minute function is the finest scale that is available.

If the measuring aperture of the tipping bucket rain gauge is small compared to the smallest spatial variation of the rain rate within a rainstorm, then, to a good approximation, the density function measured by the tipping bucket is a point function. In terms of the model storm cell it is seen that a non-zero rain rate is measured only when the center of a storm cell occurs within a circle with the same diameter as the storm cell, d(r) centered at the bucket. Since the occurrence of storm centers is uniform over the universe of storm center locations, the probability that a storm center occurs within this circle is proportional to the ratio of the area of this circle, $A_B(r)$, to the area of an unknown universe, A_u, in which storms are assumed to occur. Thus, the probability that a storm center occurs in $A_B(r)$ is

(26) $p(\text{storm in } A_B) = A_B(r)/A_u.$

It follows that the tipping bucket rain rate probability density function in terms of the model storm cell rain rate probability density function is

(27) $p_B(r) = p_r(r)\ A_B(r)/A_u.$

Due to the physical nature of the precipitation process, the function $p_B(r)$ has two components. The first, $p_B'(r)$ is the probability density of a non-zero rain rate r in $A_B(r)$. The second is $p_{Bo}\delta(r)$ which is the probability density of no cell center in $A_B(r)$.

Substituting these components for $p_B(r)$ in Eq. (27) and solving for $p_r(r)$ the result is

(28) $p_r(r) = [p_B'(r) + p_{Bo}\delta(r)]\ A_u/A_B(r).$

The probability distribution function $P_\ell(\ell_1(\alpha_o,r))$ is determined from the storm cell propagation path intersection geometry. The area in which a storm cell center can occur and intersect the propagation path over a length $\ell_1(\alpha_o,r)$ is denoted by $A(\ell_1(\alpha_o,r))$; then the probability function $p_\ell(\ell_1(\alpha_o,r))$ is given by

(29) $P_\ell(\ell_1(\alpha_o,r)) = A(\ell_1(\alpha_o,r))/A_u.$

Substituting Eqs. (28) and (29) into (24) yields

$$(30) \quad P_\alpha(\alpha_o) = N \int_{r_{min}(\alpha)}^{\infty} [p_B'(r) + p_{Bo}(r)\,\delta(r)]\, A(\ell_1(\alpha_o,r))/A_B(r)dr.$$

The constant N found from Eq. (25) is

$$(31) \quad N = 1/\left[p_{Bo}A(\ell_1(0,0))/A_B(0) + \int_0^{\infty} p_B'(r)A(\ell_1(0,r))/A_B(r)dr\right].$$

The propagation path - storm cell intersection can occur in one of four ways. The path can enter the cell side and exit through a cell side or through the cell top. On the other hand, the path can originate from within the cell and exit through the cell top or cell side. Horizontal and vertical views of each of these four cases are shown in Fig. 3.

The boundaries of the area $A(\ell_1(\alpha_o,r))$ are determined by the condition that the intersection of the storm cell and the propagation path equals or exceeds a specified length. The restrictions on the cell center location (x_o,y_o) are determined from the equations which describe the intersection of the propagation path and the storm cell. It is noted first that a necessary condition, which must be met, is that the intersection path length specified by $\ell_1(\alpha_o,r)$ be shorter than the longest possible intersection path for any cell location. The maximum intersection path is shown in Fig. 4 for the two exit cases. In Fig. 4a it is seen that the maximum intersection length, ℓ_{max}, is determined by the cell diameter, d(r) and the elevation angle, ξ. For this case ℓ_{max} is given by

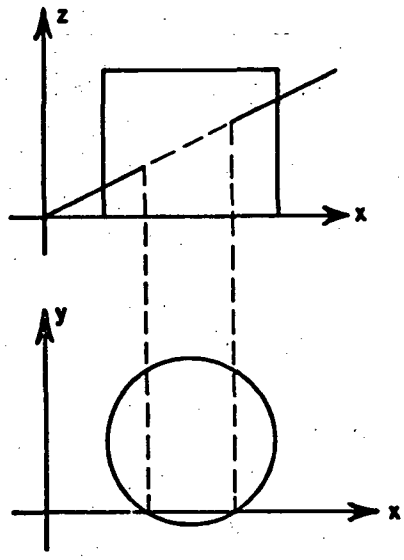

Case a. Side-side cell-path intersection

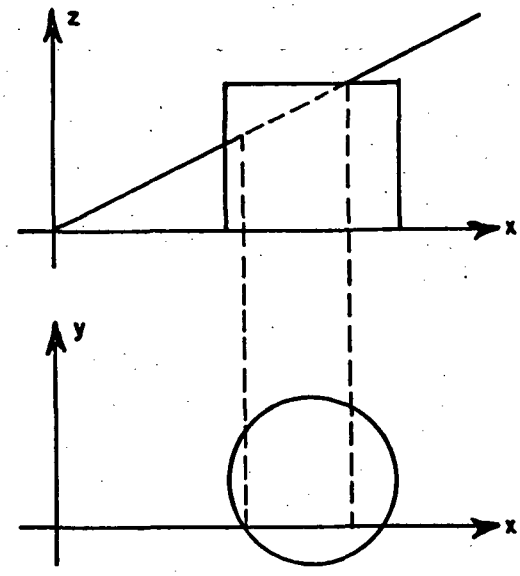

Case b. Side-top cell-path intersection

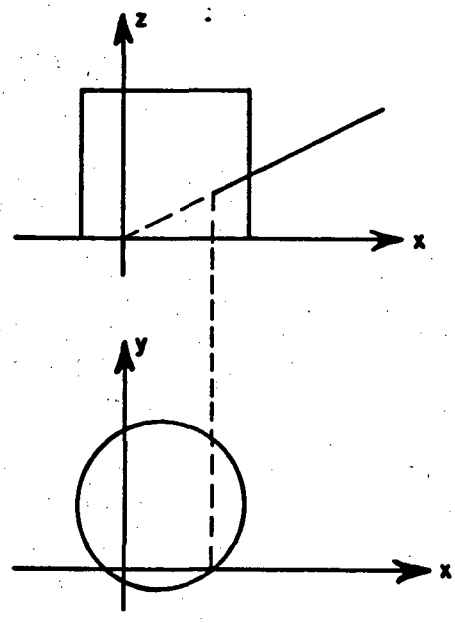

Case c. Interior-side cell-path intersection

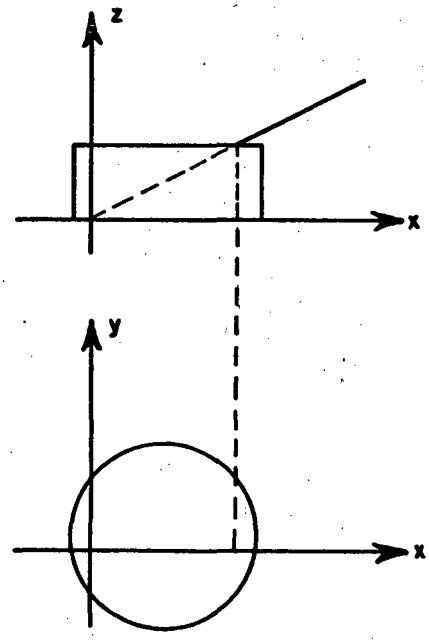

Case d. Interior-top cell-path intersection

Fig. 3.--Cell-path intersections for a single site.

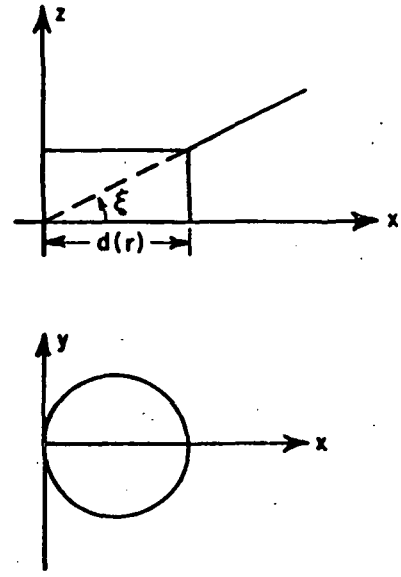

(a)

Maximum path intersection length determined by the cell diameter.

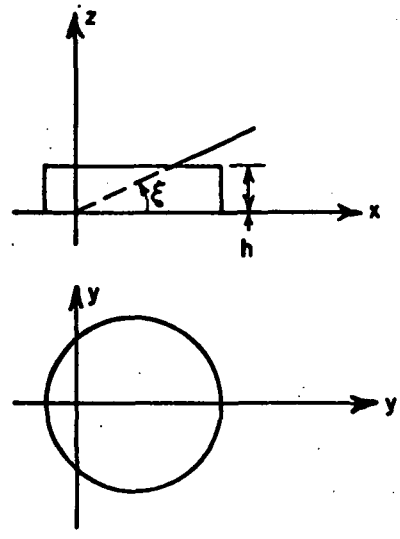

(b)

Maximum path intersection length determined by the cell height.

Fig. 4.--Maximum path intersection lengths.

(32) $$\ell_{max} = d(r)/\cos \xi.$$

The maximum length, ℓ_{max}, for the top exit case is determined by the height, h, and elevation angle, ξ, as

(33) $$\ell_{max} = h/\sin \xi.$$

Thus, given ℓ_1, the first condition which must be met is

(34) $$\ell_1 \leq \text{minimum } (d(r)/\cos \xi, h/\sin \xi).$$

Otherwise, $A(\ell_1(\alpha_o,r))$ is zero.

Assuming this condition has been met, the intersections shown earlier in Fig. 3 can be considered. For cases (a) and (b) the earth terminal is outside the storm cell so that the propagation path enters the storm cell side. Thus, the storm center must lie outside the circle given by Eq. (35).

(35) $$x_o^2 + y_o^2 = R^2.$$

For these calculations, the rain rate, r, will be assumed to be constant and the cell radius will be represented as R to simplify the notation. In case (a), the propagation path exits the side of the storm. For the intersection points to lie on the circular boundary of the cell, the x coordinate of the center, x_o, must be located outside the circle given by

(36) $$(x_o - h/\tan \xi)^2 + y_o^2 = R^2.$$

The case (b) intersection shows the propagation path exiting the storm cell through the top. The conditions on the storm center location for this intersection require that x_o lie within the circles

(37) $$(x_o - (h/\tan \xi - \ell_1 \cos \xi))^2 + y_o^2 = R^2$$

and

(38) $$(x_o - h/\tan \xi)^2 + y_o^2 = R^2.$$

Substituting these conditions on x_o into Eq. (35) the restriction that y_o must lie between the lines

(39) $$y_o = \pm \sqrt{R^2 - (\ell_1^2 \cos^2 \xi)/4}$$

results.

The boundaries for the storm center locations for cases (c) and (d) are determined in a similar fashion. For these cases, the earth terminal must be contained in the storm cell, so the center (x_o, y_o) must lie within the circle

(40) $$x_o^2 + y_o^2 = R^2.$$

For the propagation path to exit through the cell side, x_o must be inside the circle

(41) $$(x_o - \ell_1 \cos \xi)^2 + y_o^2 = R^2$$

and outside the circle

(42) $$(x_o - h/\tan \xi)^2 + y_o^2 = R^2.$$

The top exit occurs when x_o lies within the circle

(43) $$(x_o - h/\tan \xi)^2 + y_o^2 = R^2.$$

As before, the limits on y_o are defined by Eq. (39).

When these conditions are combined the region where a storm center may be located and intersect the propagation path is bounded by the solid line shown in Fig. 5. The cross-hatched area is the

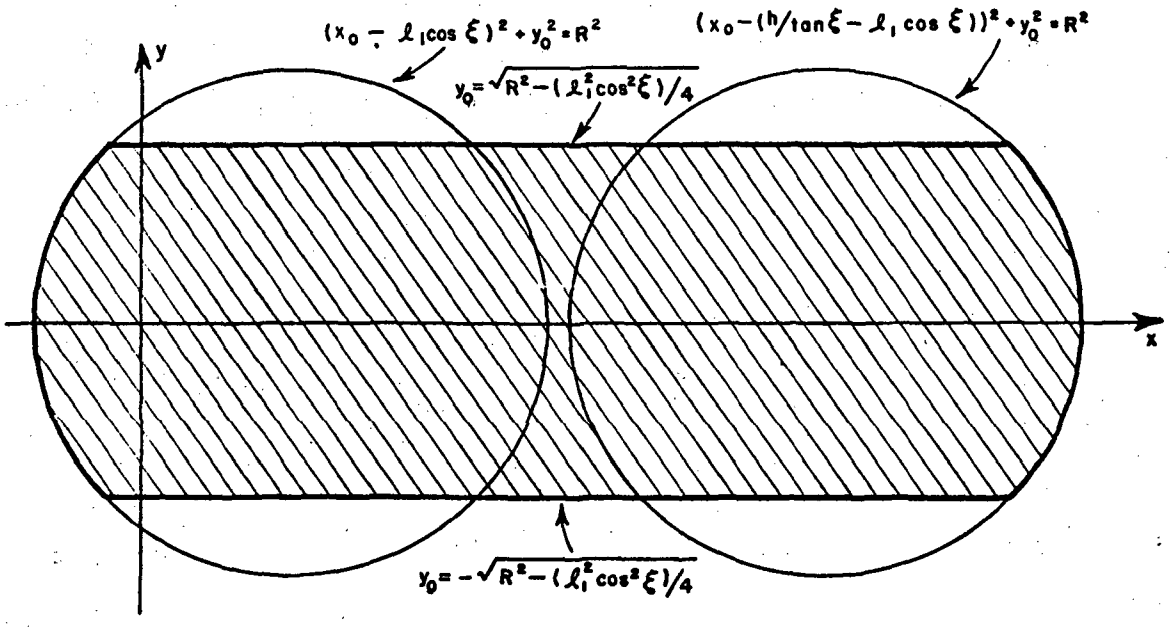

Fig. 5.--Area for storm cell-propagation path intersection length $\geq \ell_1$ for a single site.

region whose area is $A(\ell_1(r,\alpha_o))$. The area contained in these boundaries is given as

$$(44) \qquad A(\ell_1(\alpha_o,r)) = \left(\frac{hD}{\tan \xi} - \frac{3\, D\ell_1 \cos \xi}{2} \right) \sqrt{1 - \frac{\ell_1^2 \cos^2 \xi}{D^2}} + \frac{D^2}{2} \sin^{-1} \left(\sqrt{1 - \frac{\ell_1^2 \cos^2 \xi}{D^2}} \right)$$

where

$$(45) \qquad D = d(r)$$

$$(46) \qquad \ell_1(\alpha_o,r) = \alpha_o / k r^p .$$

Recalling Eq. (30)

$$(30) \qquad P_\alpha(\alpha_o) = N \int_{r_{min}(\alpha_o)}^{\infty} [p_B'(r) + p_{Bo}\delta(r)]\, A(\ell_1(\alpha_o,r))/A_B(r)dr$$

it is seen that the attenuation probability distribution function has been calculated for a single earth terminal which is effected by a single model storm cell intersecting the propagation path. In the next chapter, the effect of a single model storm cell on two spatially separated earth terminals will be considered.

CHAPTER III
CALCULATION OF THE TWO TERMINAL JOINT ATTENUATION PROBABILITY DISTRIBUTION

In the previous chapter the single terminal attenuation probability distribution function was calculated using a cylindrical storm cell model. This same storm cell model can also be used to calculate the two terminal joint attenuation probability distribution function due to a single storm cell. If the spatial separation is not too large the intersection of the two propagation paths by two different cells is not likely and thus a single cell model is all that is needed. For this calculation the same storm cell model used in Chapter II will be used by assuming that this single storm cell affects both terminals simultaneously.

To calculate the probability that the attenuations observed at both terminals simultaneously equal or exceed the attenuation, α_o, denoted as $P_{2\alpha}(\alpha_o)$, the procedure used earlier to calculate $P_\alpha(\alpha_o)$ is used again. Since the only difference in the calculation is the simultaneous propagation path intersection condition, Eq. (21) can be used directly to calculate $P_{2\alpha}(\alpha_o)$ if the definition for the path intersection probability, $P_\ell(\ell_1(\alpha_o,r))$, is changed. If the attenuation observed at both sites equals or exceeds, α_o then the model storm cell must intersect both propagation paths in such a manner that

both of the intersection path lengths equal or exceed $\ell_1(\alpha_o,r)$. With this new definition for $P_\ell(\ell_1(\alpha_o,r))$ it is seen that $P_{2\alpha}(\alpha_o)$ is

$$P_{2\alpha}(\alpha_o) = N \int_{r_{min}(\alpha)}^{\infty} [p'_B(r) + p_{Bo}\delta(r)]\, P_{2\ell}(\ell_1(\alpha_o,r))\, A_u/A_B(r)\, dr \tag{47}$$

where

$P_{2\ell}(\ell_1(\alpha_o,r))$ = probability distribution function that both propagation paths are intersected over a length equal to or exceeding $\ell_1(\alpha_o,r)$, simultaneously. (48)

As before, $P_{2\ell}(\ell_1(\alpha_o,r))$ is given by

$$P_{2\ell}(\ell_1(\alpha_o,r)) = A_2(\ell_1(r,\alpha_o))/A_u \tag{49}$$

where $A_2(\ell_1(r,\alpha_o))$ is the area where the storm center may be located such that the storm cell intersects both propagation paths over a length equal to or exceeding $\ell_1(\alpha_o,r)$, simultaneously. Since $A(\ell_1(\alpha_o,r))$ is the area where the storm cell intersects a single path over length $\ell_1(\alpha_o,r)$, then the overlap area of these single path intersection areas is the area, $A_{2\ell}(\ell_1(\alpha_o,r))$. A typical case is shown in Fig. 6. Because of the symmetry of the areas, $A(\ell_1(\alpha_o,r))$,

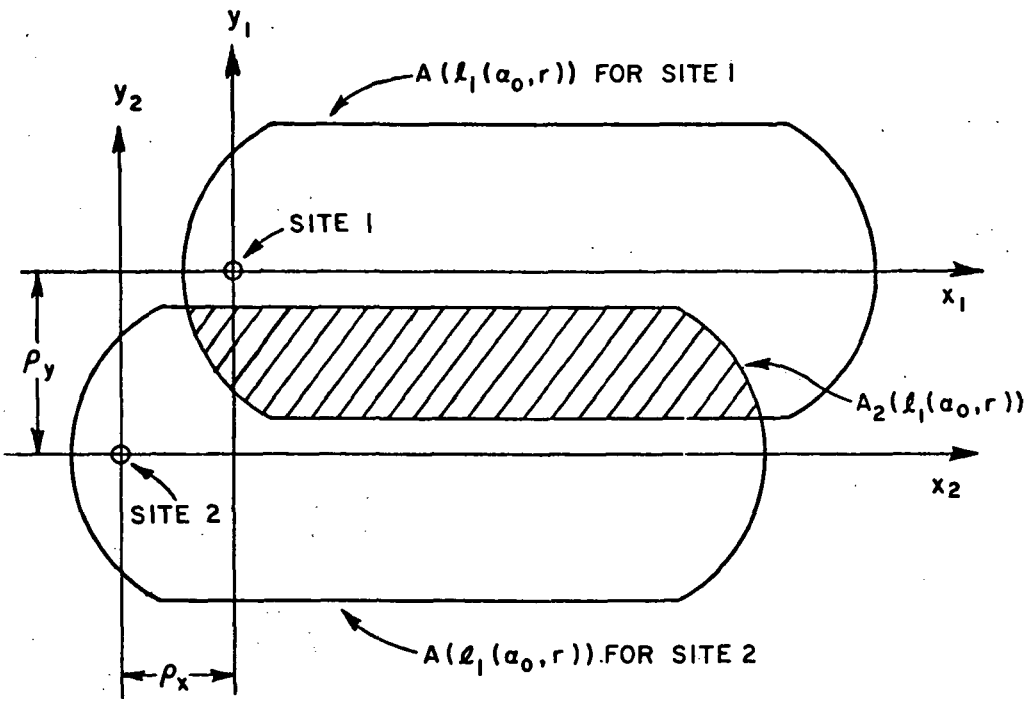

Fig. 6.--Overlap areas for two site probability distribution calculation.

for each terminal it is only necessary to consider the case where site one is located at the origin and site two is located in the third quadrant as shown in Fig. 6. The calculation of the overlap area is straightforward since boundaries of the intersection areas are known from the single terminal calculation. Thus, it is necessary only to identify the various overlap cases, calculate the boundary intersections, and evaluate the area. In calculating the overlap area it is assumed that site 2 is separated from site 1 by a distance ρ_x in the x direction and ρ_y in the y direction. These separation dimensions are also shown in Fig. 6.

Due to the circular shape of the cell model, portions of the overlap area are truncated circular segments like the shaded area in Fig. 7. To simplify the equations for $A_{2\ell}(\ell_1(\alpha_o,r))$ the function $A_s(x_1,x_2,w)$ will be defined in Eq. (50).

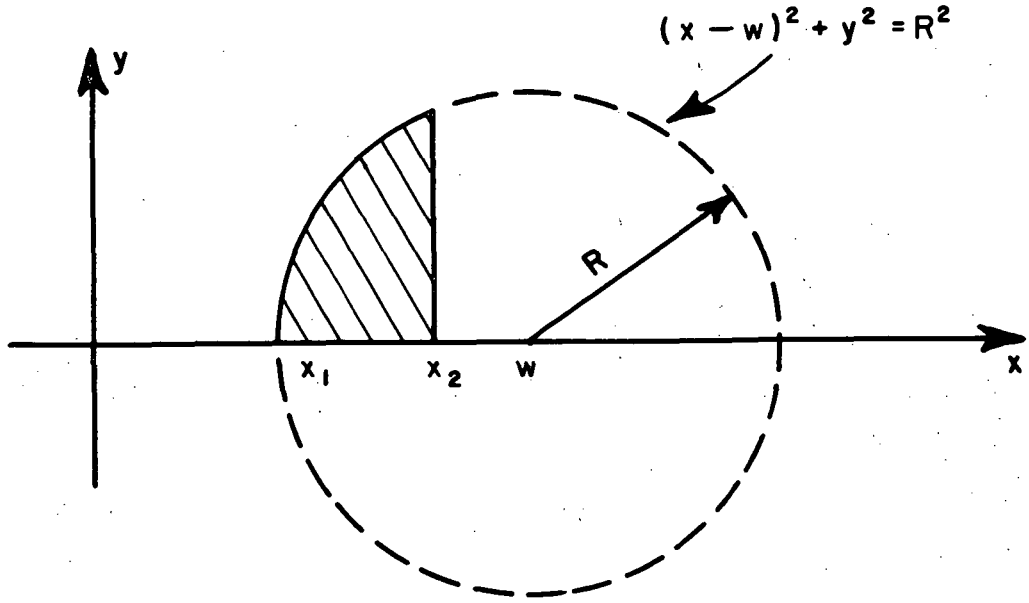

Fig. 7.--Truncated circular segment.

$$A_s(x_1,x_2,w) = \int_{x_1}^{x_2} \sqrt{R^2-(x-w)^2}\, dx. \tag{50}$$

In the remaining calculations, the dependence of $A_s(x_1,x_2,w)$ on the cell radius, R, will be understood. To further simplify the equations the following quantities will be used

(51a) $a = h/\tan \xi - \ell_1 \cos \xi$

(51b) $b = \ell_1 \cos \xi$

(51c) $c = a + \rho_x$

(51d) $d = b + \rho_x$

(51e) $e = 1/2 \sqrt{d^2 - b^2}$

(51f) $f = e + \rho_y$

(51g) $g = \rho_y$

(51h) $h' = h/\tan \xi$

(51i) $\ell' = \ell_1 \cos \xi$.

Substituting into the boundary equations determined earlier for $A(\ell_1(\alpha_0, r))$ in Eqs. (34)-(42) the boundaries for the typical overlap shown in Fig. 8 are obtained. Since the relative positions of the

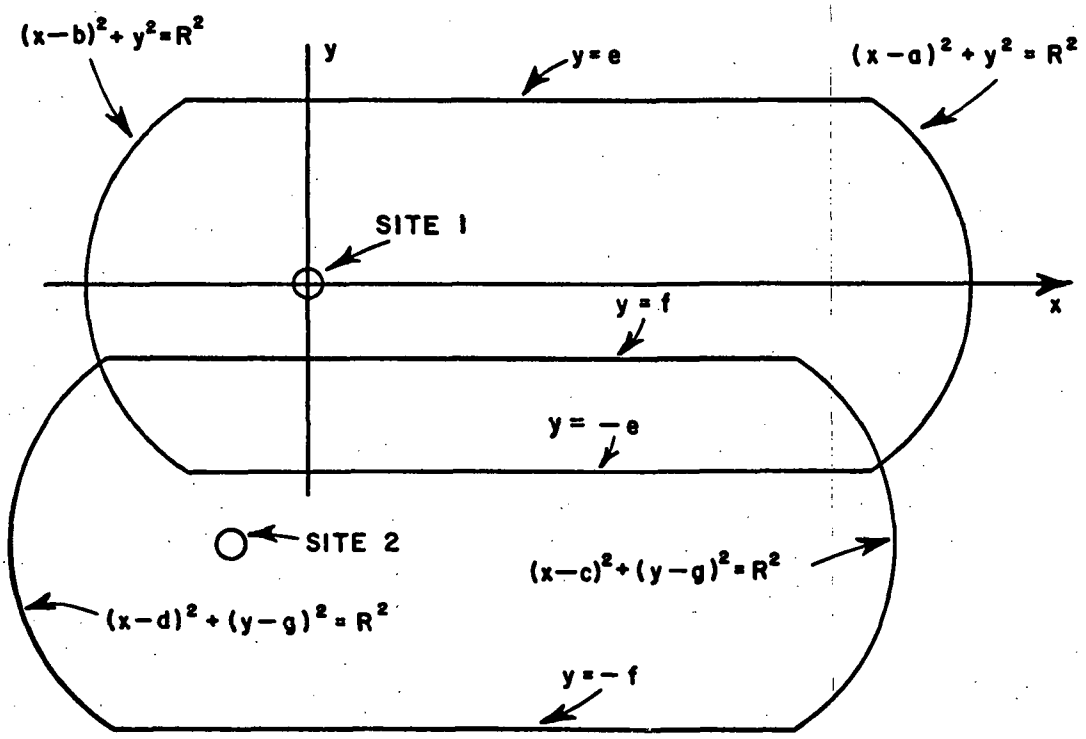

Fig. 8.--Influence area boundary equations.

influence areas will remain the same for all cases to be shown, these equations will not be shown on later figures of the overlap cases.

As the placement of the second site is varied in the third quadrant eight cases must be considered and these are shown in Fig. 9. For each case the intersection points are identified along with other pertinent points when space and clarity permit. The intersection points were calculated for the eight cases and the conditions for that type of intersection determined. The overlap areas were then broken into subareas and the subareas calculated. The total area is the arithmetic sum of the subareas. The case numbers, points used in the subarea calculations, intersection restrictions, and subareas are presented in Table 1. To calculate $P_{2\ell}(\ell_1(\alpha_0,r))$ the intersection points are calculated and the appropriate case chosen from Table 1. The subarea equations are then used to calculate $A_2(\ell_1(\alpha_0,r))$. In conclusion, using Eq. (47) and the appropriate equations from Table 1 it is possible to calculate the joint attenuation distribution for two spatially separated terminals.

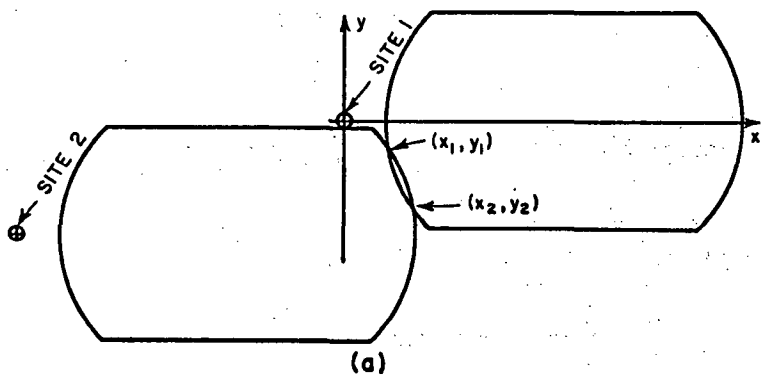

Fig. 9a.--Two site intersection area, Case I.

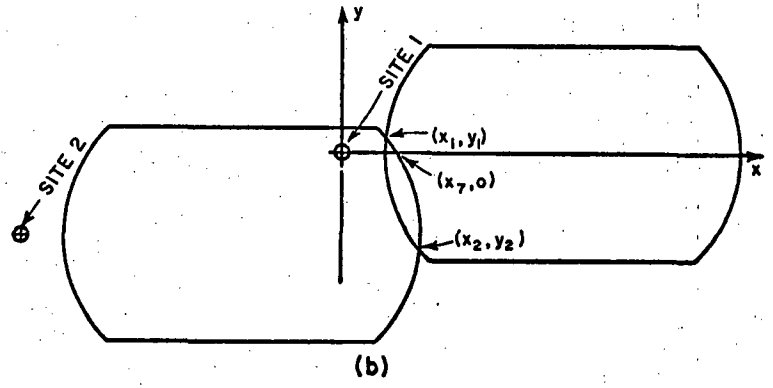

Fig. 9b. Two site intersection area, Case II.

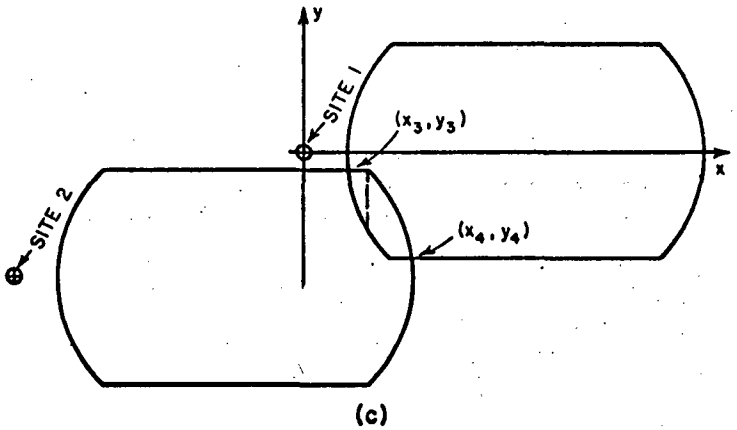

Fig. 9c.--Two site intersection area, Case III.

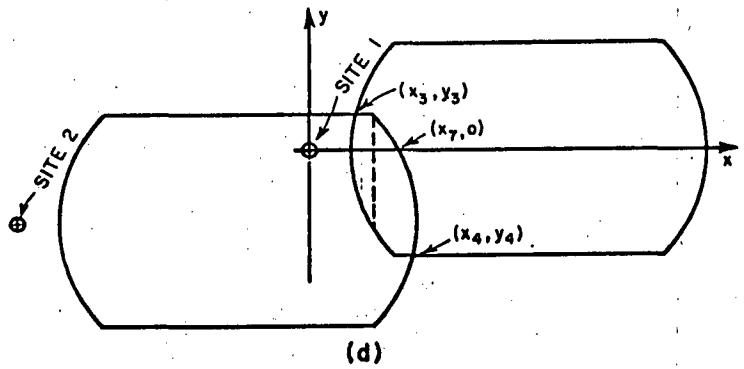

Fig. 9d.--Two site intersection area, Case IV.

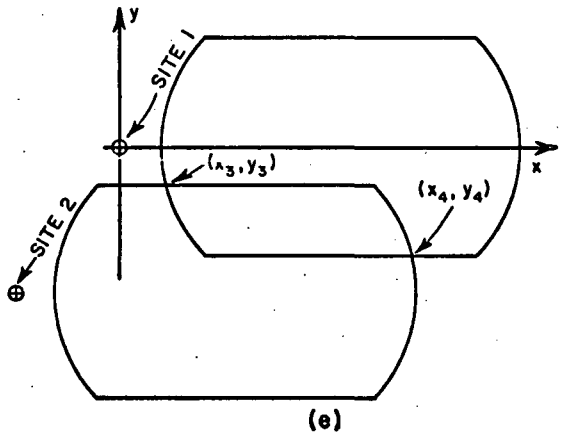

Fig. 9e.--Two site intersection area, Case V.

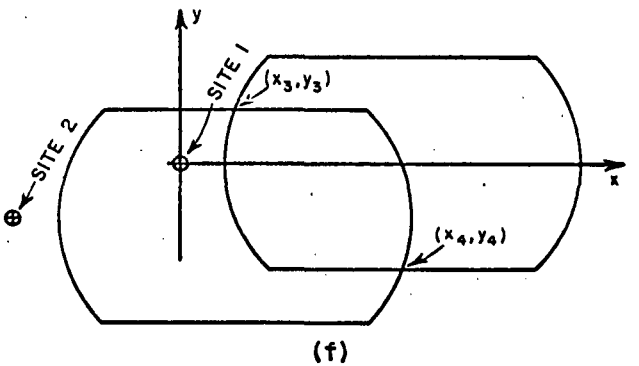

Fig. 9f.--Two site intersection area, Case VI.

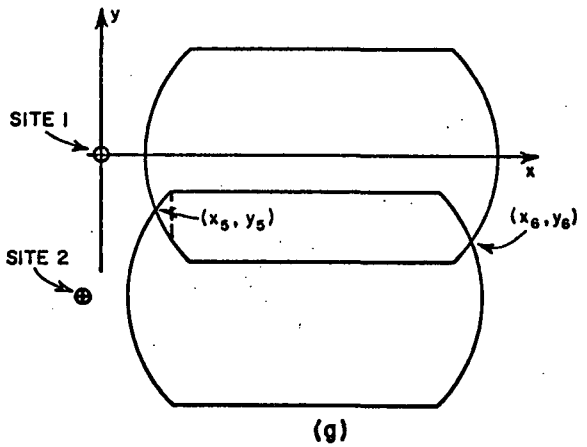

Fig. 9g.--Two site intersection area, Case VII.

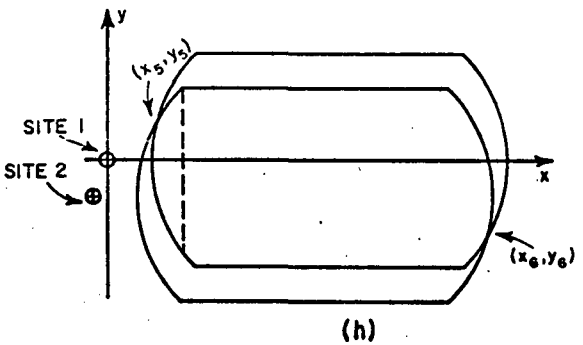

Fig. 9h.--Two site intersection area, Case VIII.

Table 1
TWO SITE INTERSECTION AREA $A_{2\ell}(\ell_1(\alpha_0,r))$

CASE	POINTS USED IN SUBAREA CALCULATION	INTERSECTION RESTRICTIONS	SUBAREAS
I	$x_{1,2} = \left(b-pq \pm \sqrt{(pq-b)^2-(1+p^2)(b^2+q^2-R^2)}\right)/(1+p^2)$	$y_1 \leq f$	$A_I = A_s(x_1,x_2,c) + (x_2-x_1)g$
	$p = (b-c)/g$	$y_1 < 0$	$A_{II} = A_s(x_1,x_2,b)$
	$q = (g^2+c^2-b^2)/2g$	$y_2 \geq -e$	
	$y_{1,2} = px_{1,2}+q$	$x_1 \geq \ell' - d/2$	
	choose sign such that $x_1>x_2$	$x_2 \leq \ell'/2$	
II	$x_7 = c + \sqrt{R^2-g^2}$		$A_I = A_s(\ell'-R,x_1,b) + g(x_7-x_1) + A_s(x_1,x_7,c)$
	$y_7 = g + \sqrt{R^2-(x_1-c)^2}$	Same as Case I with the additional condition	$A_{II} = A_s(\ell'-R,x_7,b) + (x_{10}-x_7)(g-y_{10}) + A_s(x_7,x_{10},c)$
	$x_8 = b - \sqrt{R^2-g^2}$		$+ (x_8-x_7)\,y_{10} + A_s(x_7,x_8,b) + (x_{10}-x_8)\,(y_{10}-\rho_y)$
	$x_9 = R + h'-\ell'+\rho_x$	$y_1 \geq 0$	$+ A_s(x_{10},x_9,c)$
	$y_{10} = -\sqrt{R^2-(x_7-b)^2}$		$A_{III} = g(x_2-x_8) + A_s(x_8,x_2,b) + A_s(x_2,x_9,c)$
	$x_{10} = c + \sqrt{R^2-(y_{10}+g)^2}$		
III	$x_3 = b - \sqrt{R^2-f^2}$	$x_3 > x_4$	$A_I = f(h'-\ell'/2+\rho_x-x_3) + A_s(x_3,h'-\ell'/2+\rho_x,b)$
	$y_3 = f$	$x_3 \geq \ell'/2$	$A_{II} = (\ell'-h'-\rho_x)g + A_s(h'-\ell'/2+\rho_x,\ell'/2,b) + A_s(h'-\ell'/2+\rho_x,\ell'/2,c)$
	$x_4 = c + \sqrt{R^2-(e+g)^2}$	$x_4 \leq h' - \ell'/2$	$A_{III} = (x_4-\ell'/2)(g+e) + A_s(\ell'/2,x_4,c)$
	$y_4 = -e$	$y_3 < 0$	

Table 1
(Contd.)

CASE	POINTS USED IN SUBAREA CALCULATION	INTERSECTION RESTRICTIONS	SUBAREAS
IV	Same as Case III	Same as Case III with the additional restrictions $y_3 \geq 0$ $x_3 \geq \ell' - d/2$	$A_I = A_s(\ell'-R, x_3, b) + f(h'-\ell'/2+\rho_x-x_3)$ $A_{II} = g(x_7-h'+\ell'/2-\rho_x) + A_s(h'-\ell'/2+\rho_x, x_7, c)$ $A_{III} = A_s(\ell'-R, x_7, b) + g(\ell'/2-x_7) + A_s(x_7, \ell'/2, b)$ $A_{IV} = A_s(x_7, h'-\ell'+R+\rho_x, c) + (x_4-\ell'/2)(e+\rho_y)$ $A_V = A_s(x_4, R+h'-\ell'+\rho_x, c) + g(R+h'-\ell'+\rho_x-x_4)$
V	Same as Case III	Same as Case III with $\ell'/2 \leq x_4 \leq h'-\ell'/2$	$A_I = A_s(x_3, \ell'/2, b) + f(\ell'/2-x_3)$ $A_{II} = (h'+\rho_x-\ell')(f+e)$ $A_{III} = A_s(h'-\ell'/2+\rho_x, x_4, e) + (x_4-h'+\ell'/2-\rho_x)(g+e)$
VI	Same as Case III	$\rho_x \geq \ell' - h'$ $x_7 \geq \ell'/2$ $x_4 \leq h' - \ell'/2$	$A_I = A_s(\ell'-r, x_3, b) + f(h'-\ell'/2+\rho_x-x_3)$ $A_{II} = A_s(h'-\ell'/2+\rho_x, x_7, c) + g(x_7-h'+\ell'/2-\rho_x)$ $A_{III} = e(x_7-\ell'/2) + A_s(\ell'-R, \ell'/2, b)$ $A_{IV} = A_s(x_7, h'-\ell'+d/2+\rho_x, c) + (x_4-x_7)(\rho_y+e)$ $A_V = A_s(x_4, h'-\ell'+d/2+\rho_x, c)$

Table 1
(Contd.)

CASE	POINTS USED IN SUBAREA CALCULATION	INTERSECTION RESTRICTIONS	SUBAREAS
VII	$x_5 = \left(b-mn \pm \sqrt{(b-mn)^2-(1+n^2)(b^2+m^2-R^2)}\right)/(1+n^2)$ $y_5 = m+nx_5$ $m = (d^2-b^2+g^2)/2g$ $n = (b-d)/g$ $x_6 = \left(a-tu+\sqrt{(a-tu)^2-(1+u^2)(a^2+t^2-R^2)}\right)/(1+u^2)$ $y_6 = t+ux_6$ $t = (c^2-a^2+g^2)/2g$ $u = (a-d)/b$	$y_5 < 0$ $x_6 \geq h' - \ell'/2$	$A_I = (\ell'/2+\rho_x-x_5)(g-y_5) + A_s(x_5,\ell'/2+\rho_x,d)$ $A_{II} = (x_6-h'+\ell'/2-\rho_x)(g-y_6) + A_s(h'-\ell'/2+\rho_x,x_6,c)$ $A_{III} = (h'-\ell'+\rho_x)(f+e) + y_5(\ell'/2-x_5) + A_s(x_5,\ell'/2,b)$ $A_{IV} = y_6(x_6-h'+\ell'/2) + A_s(h'-\ell'/2,x_6,a) - \rho_x(y_6+e+f-y_5)$
VIII	Same as Case VII	$y_5 < 0$ $x_6 \geq h' - \ell'/2$	$A_I = (\ell'-R,x_5,b) + g(\ell'/2+\rho_x-x_5) + A_s(x_5,\ell'/2+\rho_x+d)$ $A_{II} = f(h'-\ell') + g(x_7-h'+\ell'/2-\rho_x) + A_s(h'-\ell'/2+\rho_x,x_7,c)$ $A_{III} = A_s(\ell'-R,\ell'/2,b) + e(h'-\ell') - y_6(x_7-h'+\ell'/2)$ $A_{IV} = A_s(x_7,R+h'-\ell'+\rho_x,c) + (x_6-x_7)(\rho_y-y_6)$ $A_V = (x_6-x_7)(\rho_y-y_6) + y_6(x_6-h'+\ell'/2) + A_s(h'-\ell'/2,x_6,a)$ $A_{VI} = A_s(x_6,R+h'-\ell'+\rho_x,c)$

CHAPTER IV
MODEL STORM CELL PARAMETERS

The attenuation probability distributions presented in the last two chapters were calculated using a cylindrical storm cell model. In this chapter storm cell height, h; storm cell diameter as a function of rain rate, d(r); and the tipping bucket rain rate probability density function, $p_B(r)$, will be discussed. These parameters are used to relate the storm cell model to real world storm phenomena.

Rain Rate Probability Density Function

The most difficult parameter to determine is the tipping bucket rain rate probability density function, $p_B(r)$, because of its temporal and geographic variability. For the storm cell model to be useful in making earth terminal design decisions, the tipping bucket rain rate probability characteristics for each earth site must be known. Currently, the most commonly available data for calculating this function are collected by the National Weather Service as mentioned earlier. The rain rates which are measured, however, are determined on a clock-hourly basis and represent the average rain rate during a sixty minute period beginning at the start of each hour. This integration time is too coarse for use here since a rain rate

of 100 mm/hr for fifteen minutes and a rain rate of 25 mm/hr for sixty minutes are measured as the same clock-hour rain rate of 25 mm/hr. The measurement that is needed is the instantaneous rain rate.

Bussey[10] made the first attempt to estimate instantaneous rain rates by empirically determining a relationship between clock-hour rain rates and instantaneous rain rates. Although his results are valid only for Washington, D.C., this approach represents a useful initial effort and has been used to estimate instantaneous rain rate statistics for other cities[11].

A study of excessive precipitation was made by Dyck and Mattice[12] in which an attempt was made to catalog the number of occurrences of rain events which produced 2.5 inches or more in 24 hours or 1.0 inch or more in one hour on a national basis. However, the data presented is much too coarse to be useful in predicting millimeter wavelength attenuation. Lenhard, Cole and Sissenwine[13] presented an algorithm for estimating the rain rates exceeded for 0.1, 0.5, 1.0 and 2.0 percent of time from the local mean temperature and a precipitation index. Although this technique gives four points on the rain rate probability curve, further detail is needed.

A rain rate probability density function, which gives a functional form for $p_B(r)$ which is geographically determined, has been postulated by Rice and Holmberg[14]. The rain rate probability distribution function was developed for twelve geographic regions in the continental United States for averaging times of one, five

and sixty minutes. Although not ideal, the clock-one minute distribution will be used here since it appears to be the finest scale presently available. Since the Rice-Holmberg rain rate probability function is used extensively in the attenuation probability function calculations it will be briefly explained here.

This rain rate probability function was derived using precipitation data from forty-nine locations in the United States, as well as fourteen other stations throughout the world. From this data Rice and Holmberg determined that the rain rate probability distribution for non-zero rain rates could be modelled by the sum of three exponential modes. The total distribution is the sum of these three modes as shown in Eq. (52)

$$P_t(r_o) = \sum_{i=1}^{3} A^j_{i,t} \exp(-r_o/B_{i,t}) \tag{52}$$

where $P_t(r_o)$ = the probability distribution that the clock-t minute rain rate, r_o, is exceeded

t = the clock averaging period

$A^j_{i,t}$ = the mode coefficient for the j^{th} region and the i^{th} mode for the clock-t period

$B_{i,t}$ = the mode rate for the i^{th} mode and clock-t period.

Since the Rice-Holmberg function is a probability distribution function the density function used in Eqs. (24) and (47) can be calculated by differentiation. It is noted that since $P_t(r_o)$ is the

probability that a non-zero rain rate r_o is exceeded the resulting density function will be for non-zero rain rates only. Thus

$$(53) \qquad p'_B(r_o) = \sum_{i=1}^{3} A^j_{i,1}/B_{i,1} \exp(-r_o/B_{i,1}).$$

It follows from Eq. (3) that the probability density of a zero rain rate is

$$(54) \qquad P_{Bo} = 1 - \sum_{i=1}^{3} A^j_{i,1}.$$

Thus, a form for $p_B(r)$ which is geographically dependent is now available. The method in which the local rain rate characteristics can be incorporated will now be explained.

The total rainfall for the observation period used in determining the $A^j_{i,t}$ can be calculated by integrating Eq. (53) over all non-zero rain rates. It is noted by Rice and Holmberg in Reference [14] that the result is independent of the clock averaging time, t. Assuming that the rain accumulation for each mode is independent of t, then the product $A^j_{i,t}\ B_{i,t}$ is a constant for all values of, t. Calculations of this product from data presented in Reference [14] shows that this is a reasonable assumption. This relationship of the total rain accumulation for each mode can be used to calculate the mode coefficients for the clock-one minute density function from the clock-hourly data published by the National Weather Service in the following way.

First, Eq. (52) is fitted, using a minimum mean square error algorithm, to the clock-hourly rain rate probability distribution calculated from National Weather Service data. Using the values for $B_{i,60}$ and $B_{i,1}$ obtained from Reference [14],

$$B_{1,60} = 10 \quad \text{mm/hr}$$
$$B_{2,60} = 3.0 \quad \text{mm/hr}$$
$$B_{3,60} = 1.0 \quad \text{mm/hr}$$
$$B_{1,1} = 35.0 \quad \text{mm/hr}$$
$$B_{2,1} = 10.5 \quad \text{mm/hr}$$
$$B_{3,1} = 3.5 \quad \text{mm/hr}$$

the clock one-minute mode coefficients are calculated from

$$A^j_{i,1} = B_{i,60}\, A^j_{i,60\ \text{calc}} / B_{i,1}. \tag{55}$$

It should also be noted that Rice and Holmberg present a complete set of coefficients for twelve geographical regions in the United States for clock one-, five-, and sixty-minute rain rates which can be used in lieu of the coefficients calculated using the above method. The above method, however, incorporates the actual precipitation characteristics for a particular site location within a geographic region and is preferred for calculating $P_{\alpha}(\alpha_0)$ and $P_{2\alpha}(\alpha_0)$. Thus, the Rice-Holmberg rain rate probability function provides a mathematically tractable function which permits the calculation of

the tipping bucket rain rate probability density function for a particular site using locally measured tipping bucket rain rate data.

Cell Diameter - Rain Rate Function

The remaining storm cell model parameters which must be specified are the diameter-rain rate relationship, d(r) and the cell height, h. Although d(r) is not directly measurable, two forms have been proposed.

The first, was inferred by Hogg[15] from sun-tracker measurements and is shown in Fig. 10. Since discrete data points are difficult to use in numeric computations an exponential function was fitted to Hogg's model using a minimum mean square error criterion and is given in Eq. (56).

$$d(r) = 11.34 \exp(-r/33) + 1.25 \text{ (km)}. \tag{56}$$

The diameter calculated from Eq. (56) is also shown in Fig. 10.

A second diameter-rain rate function, recommended by CCIR and discussed by Benoit[15], is the logrithmic relationship given below.

$$d(r) = 41.4\text{-}23.5 \log_{10}(r) \text{ (km)}. \tag{57}$$

This model has two problems. First, for small rain rates the cell diameter approaches infinity. Second, the cell diameter becomes negative for rain rates exceeding 58 mm/hr. To prevent this from occurring in the numeric calculations, the minimum cell diameter

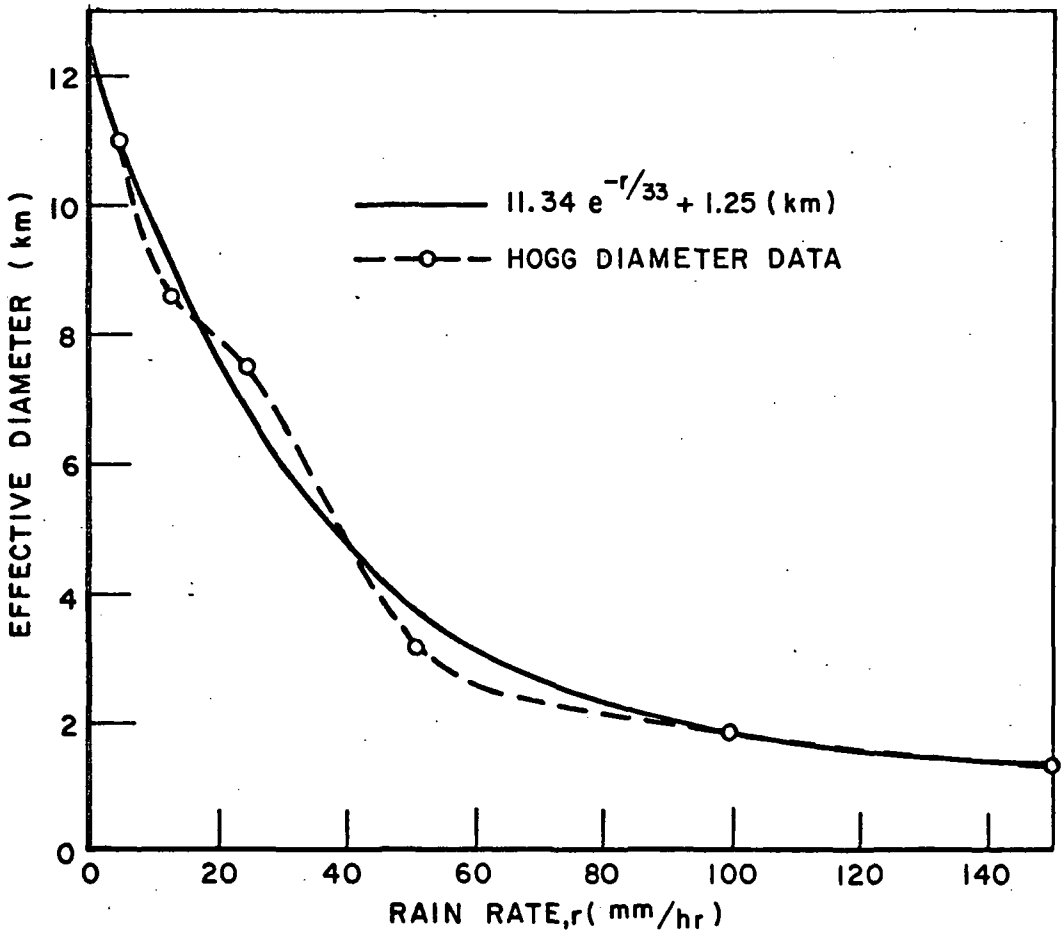

Fig. 10.--Diameter versus rain rate relationship from Reference [12].

was clamped at 1.25 km. This value was chosen based on the minimum cell diameter calculated from Hogg's model. A comparison of the exponential model and the modified CCIR model is shown in Fig. 11.

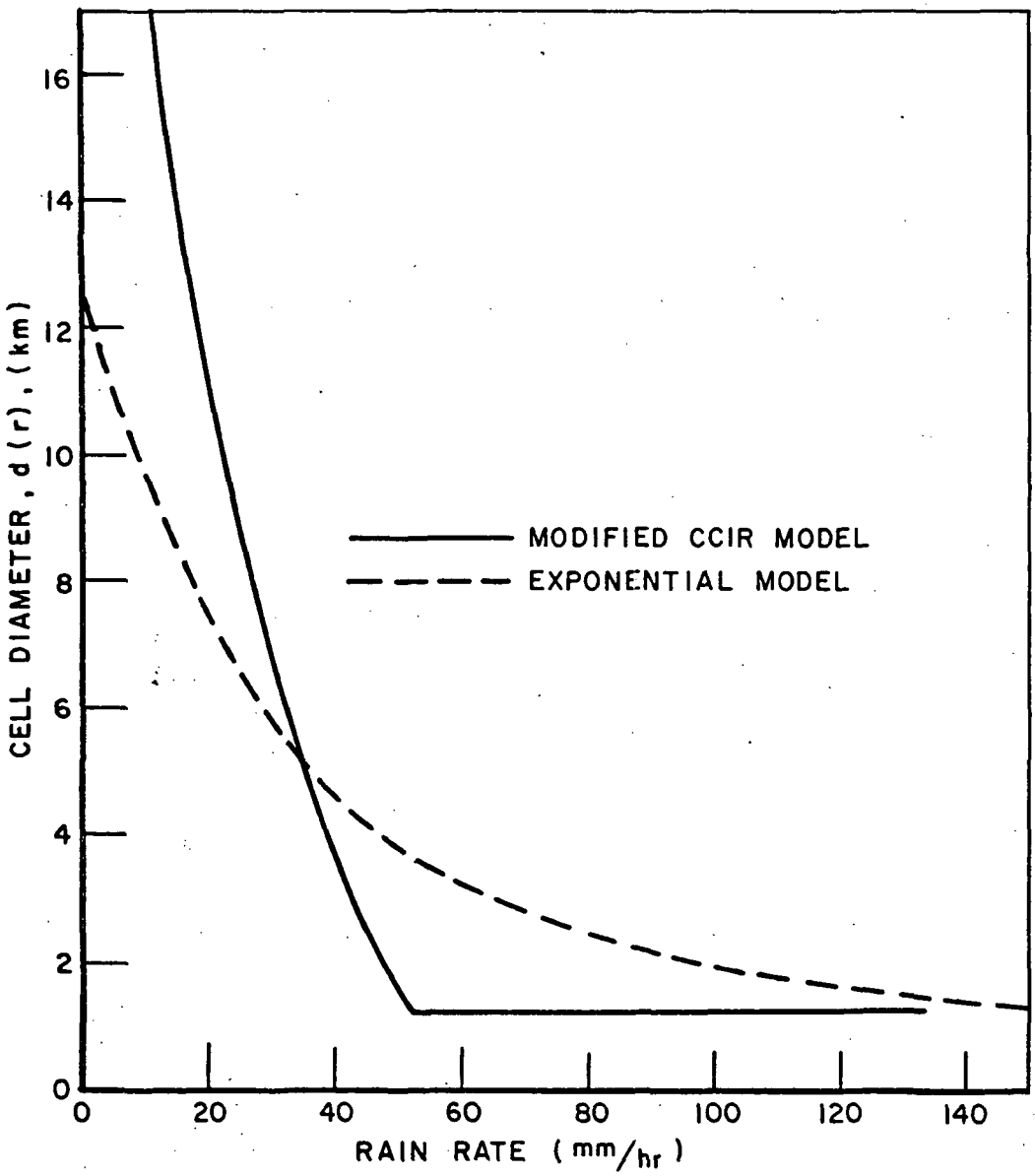

Fig. 11.--Comparison of two rain rate diameter relationships.

Cell Height

The remaining cell parameter, h, specifies the height of the attenuating region within the cell. Although, rainstorms have tops tens of thousands of feet in the atmosphere, the liquid precipitation is confined to the region below the zero degree isotherm. This isotherm represents the altitude at which precipitation is turning from solid to liquid form. Several estimates of this height have been made and will be discussed here. The first of these was a study of thunderstorms in Florida and Ohio[17]. From graphical data presented in this study, an average cell height appears to be approximately 6 km. Another source, the CCIR, recommends that a cell height of 7 km be used for temperate climates[15], and a paper recently presented by Crane[18] on backscatter due to rain used cell heights of 15 km in Florida, 11 km in New England and 7 km for the Pacific Northwest, California and the desert. It will be seen later from calculations of the attenuation probability distribution that the results are relatively insensitive to variations in the cell height and, hence, this parameter is not considered to be critical. The values used in later calculations will be specified for each case.

Attenuation-Rain Rate Relation

A final relationship which must be considered is the attenuation-rain rate relationship used in Eq. (5) and repeated below.

$$\alpha = kr^{p}\ell \tag{5}$$

where

k and p are frequency dependent constants

ℓ = path length through precipitation in km

r = rain rate in mm/hr

α = observed attenuation in dB.

Calculations and measurements of k and p can be found in References [3], [5], [7], [15], [19], [20] and [21] with a diversity of numerical values. The summary of results prior to 1965 presented by Medhurst[19] showed an 8 dB variation in the calculated attenuation for a rain rate of 100 mm/hr. A comparison of several results by Ippolito[21] resulted in his choosing k = .035 and p = 1.155 at 15.3 GHz. Interpolating data presented by Crane[20] from measurements of 4741 rain drop size distributions yields $p \simeq 1.10$ and $k \simeq .035$. This value will be used for calculations presented in the next chapter.

Summary of Parameters

Concluding, then, the parameters which will be used in the attenuation probability calculations in the next chapter are

(58) $$p_B(r) = \sum_{1}^{3} A^j_{i,1}/B_{i,1} \exp(-r/B_{i,1}),$$

where $A^j_{i,1}$ and $B_{i,1}$ are chosen from Ref. [14] or from measured rain rate data if available

(59) $$d(r) = 1.250 + 11.340 \exp(-r/33) \text{ (km)}$$

or

$$d(r) = \begin{cases} 41.4\text{-}23.5 \log_{10}(r)(\text{km}) & r \leq 52 \text{ mm/hr} \\ 1.250 \text{ km} & r > 52 \text{ mm/hr} \end{cases} \tag{60}$$

$$h = 6000 \text{ m to } 17000 \text{ m} \tag{61}$$

$$\alpha = .035\ r^{1.10}\ \ell(\text{dB}). \tag{62}$$

CHAPTER V
COMPARISON OF CALCULATED AND EXPERIMENTAL RESULTS FROM ATS-5

Attenuation probability distribution functions have been calculated in earlier chapters for one and two terminal configurations using a cylindrical storm cell model. In this chapter the results of measurements made using the Applications Technology Satellite, ATS-5, 15.3 GHz downlink at two locations will be compared to storm cell model calculations incorporating the storm cell parameters presented in the previous chapter. For both cases considered instantaneous rain rate data was available and was used to calculate the Rice-Holmberg distribution coefficients. Also presented in this chapter are discussions of the sensitivity of the results to a ± 10 percent variation in the numerical value of the parameters and a three mode exponential diameter-rain rate function.

Two ATS-5 receiving stations were considered. The first station is located at the Ohio State University in Columbus, Ohio, and consists of two terminals separated by

$$\rho_x = -2.74 \text{ km}$$
$$\rho_y = -2.99 \text{ km}$$

which yields an intersite spacing of approximately 4.0 km. The terminals are discussed in References [22] and [23] and the data

acquired in 1970 which is used here is discussed in Reference [24]. The instantaneous rain rate data was extracted from recording tipping bucket rain gauge charts and the Rice-Holmberg coefficients calculated. The second station considered was located in Rosman, North Carolina, and was operated by NASA Goddard Space Flight Center. The measured data were analyzed by the Westinghouse Corporation[25] for the 1970 data period and consists of attenuation data and instantaneous rain rate data taken during attenuation measurements. A Rice-Holmberg rain rate distribution was determined from this instantaneous rain rate data for use in the attenuation calculations.

The measured rain rate distribution and the Rice-Holmberg model for the Ohio State University data are shown in Fig. 12. The

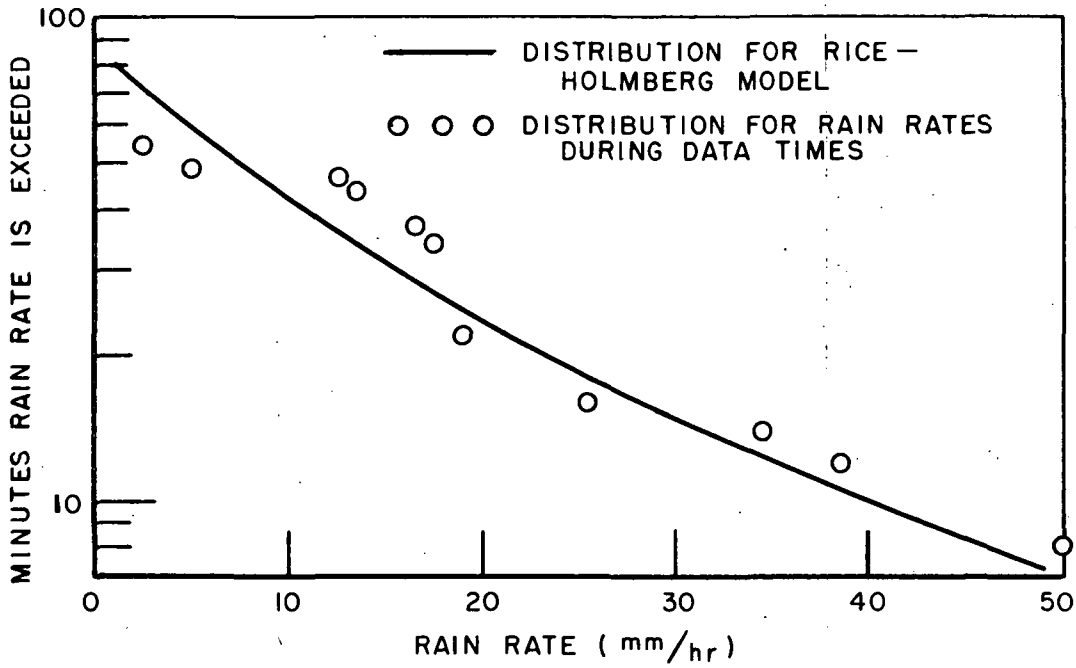

Fig. 12.--Rain rate distribution at Ohio State University during ATS-5 Data Periods in 1970.

measured and calculated attenuation probability distribution functions for the 1970, Ohio State University single terminal and diversity terminal, ATS-5 measurements are shown in Figs. 13 and 14.

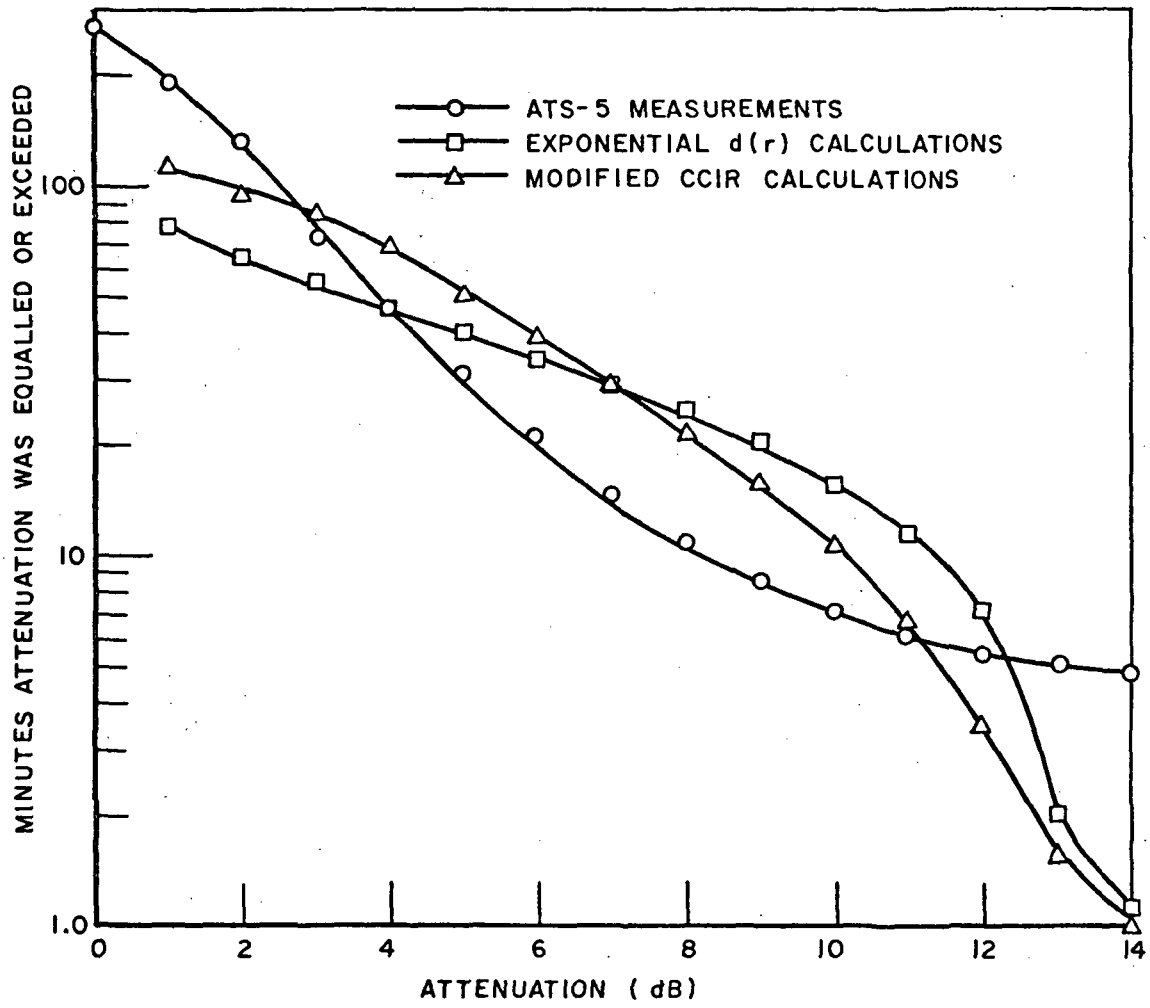

Fig. 13.--Ohio State University ATS-5 single site measured and calculated attenuation distribution.

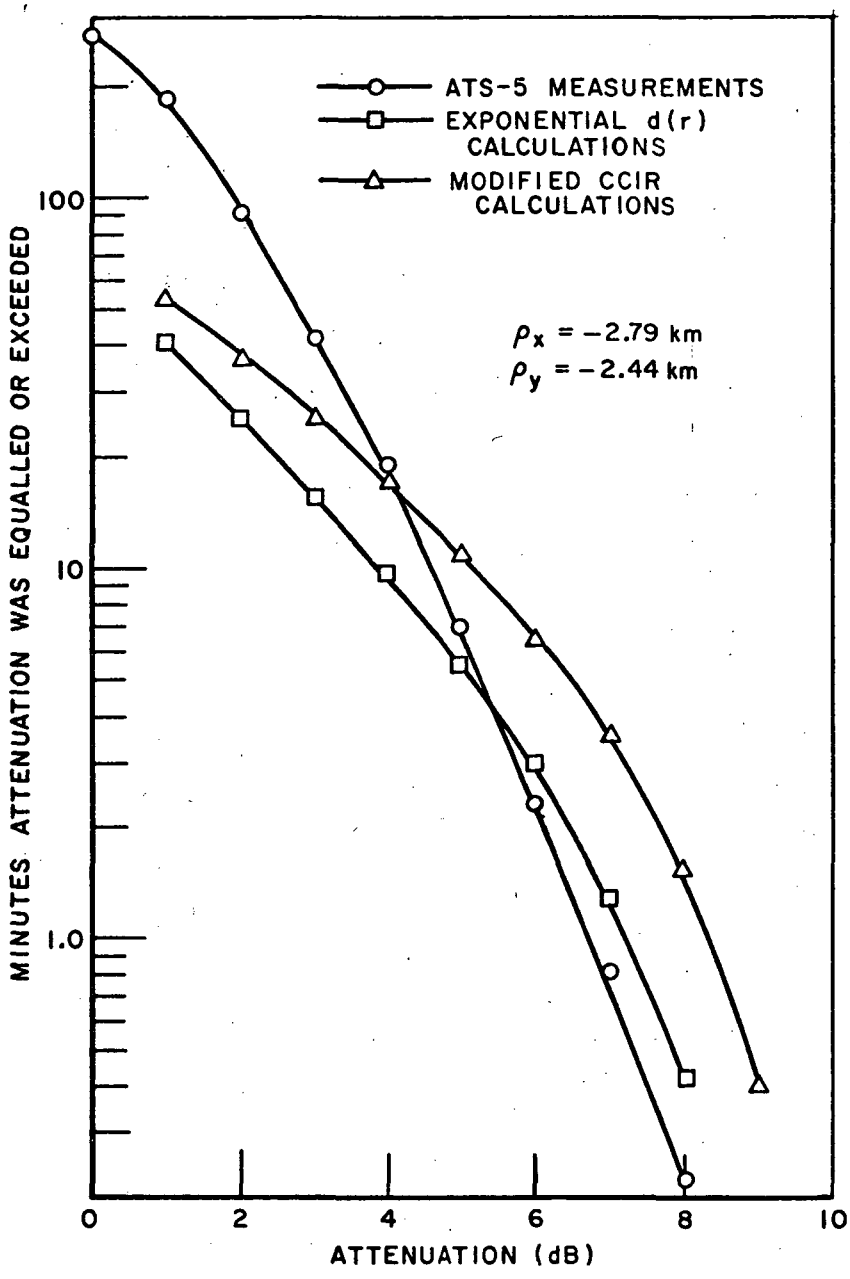

Fig. 14.--Ohio State University 1970 diversity site measured and calculated joint distribution.

Both the exponential diameter function and the modified CCIR function were used in the calculations and each distribution is shown.

Two additional quantities, the diversity improvement, $\eta(\alpha_o)$ and the diversity gain, $G(\alpha_o)$, which are defined in Eqs. (63) and (64) are shown in Figs. 15 and 16 respectively.

(63) $$\eta(\alpha_o) = P_\alpha(\alpha_o)/P_{2\alpha}(\alpha_o)$$

(64) $$G(\alpha_o) = \alpha_o - \alpha_1$$

where $$P_\alpha(\alpha_o) = P_{2\alpha}(\alpha_1).$$

From these figures it is seen that calculations using the storm cell model agree fairly well with experimental measurements. This general agreement is also seen in calculations using the NASA Rosman instantaneous rain rate data shown in Fig. 17. The calculated and measured attenuation probability distributions are shown in Fig. 18.

The agreement between the calculated and measured attenuation distributions is summarized in Fig. 19 for the exponential diameter function and the modified CCIR diameter function in Fig. 20. The error shown is the difference between the calculated attenuation and the measured attenuation for a given value of $P_\alpha(\alpha_o)$. Thus, this error is the horizontal distance between the experimental and calculated curves. It is seen in this figure that the error curves have a similar nature and range from -3 dB to +3 dB. The magnitude of the error is encouraging and shows that the storm cell model technique for predicting

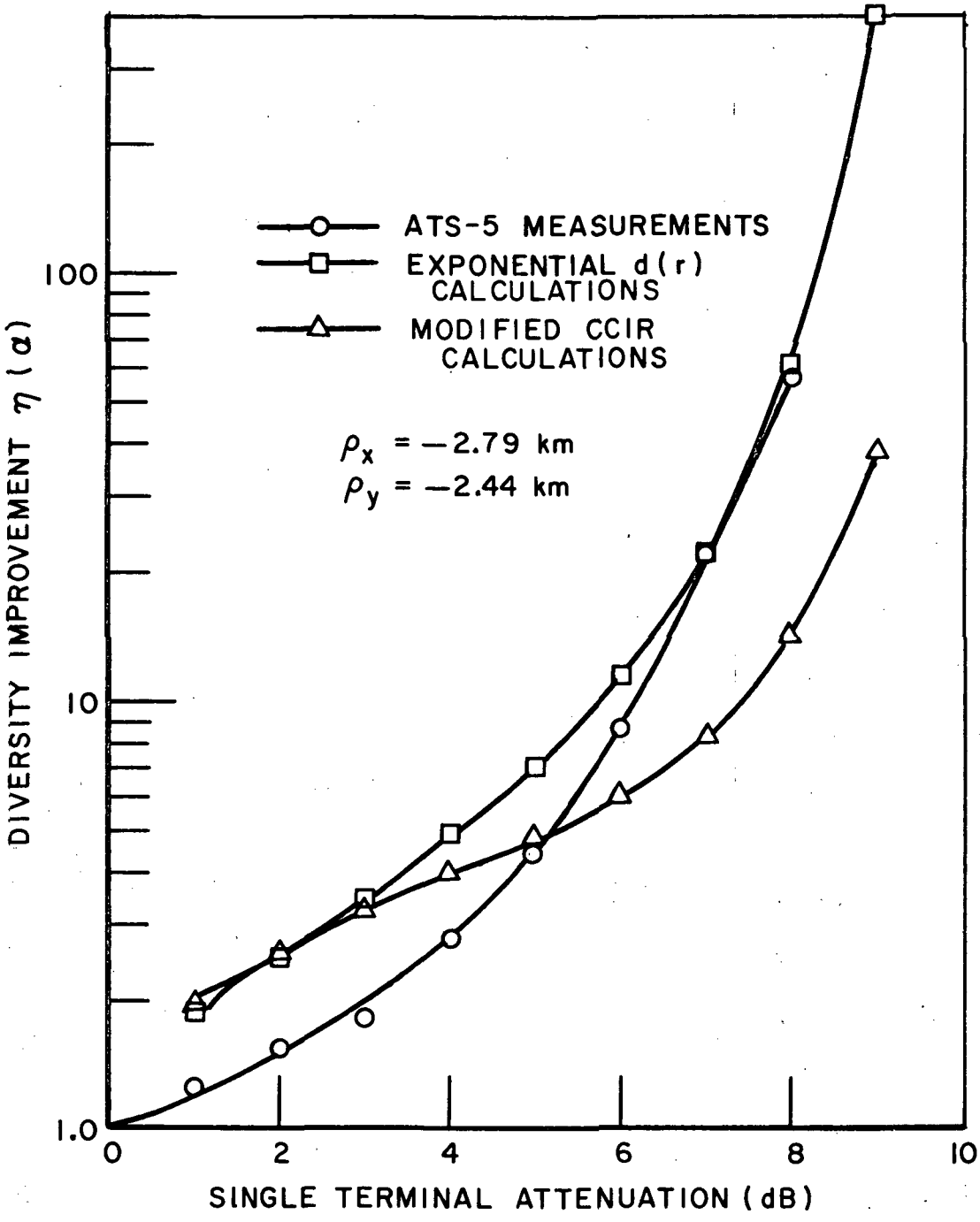

Fig. 15.--Diversity improvement for Ohio State University ATS-5 1970 diversity data.

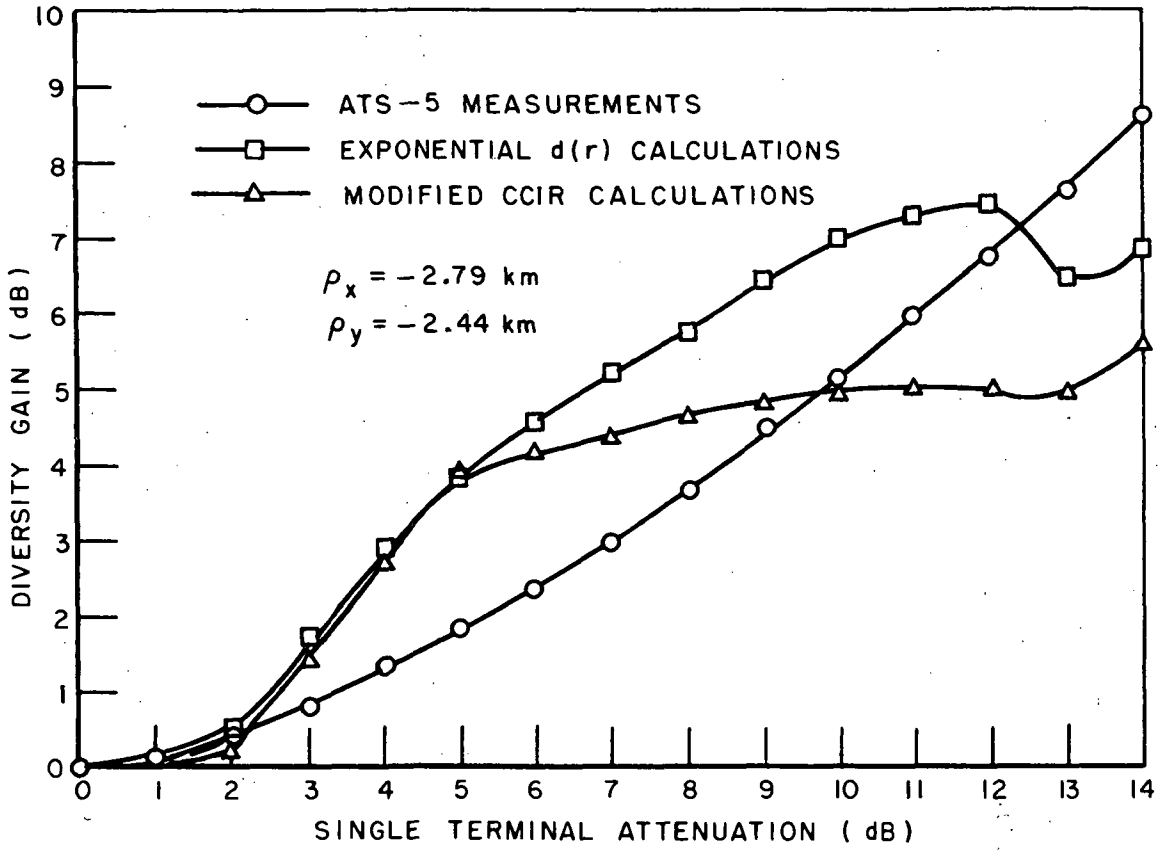

Fig. 16.--Diversity gain for Ohio State University ATS-5 1970 diversity data.

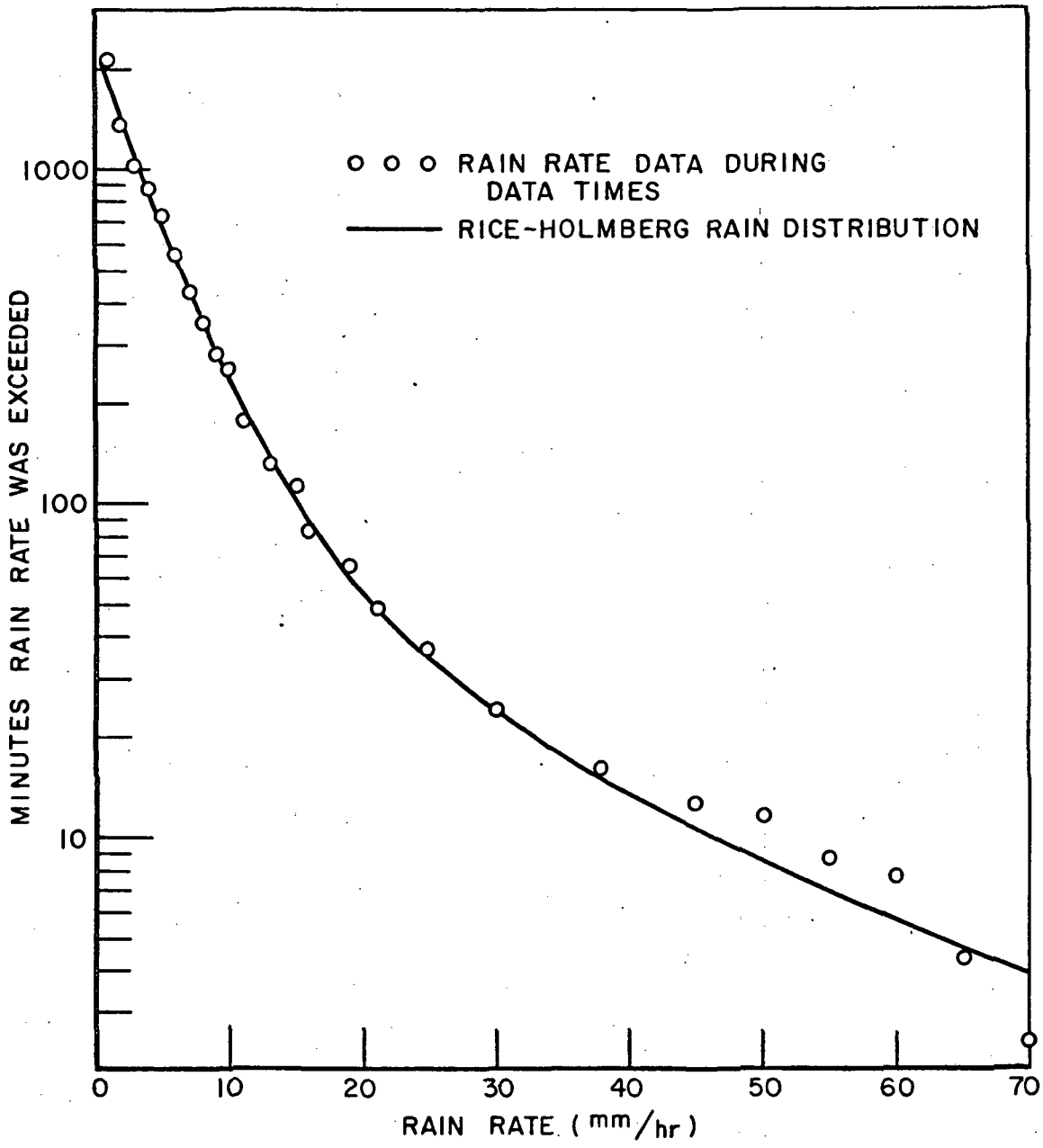

Fig. 17.--Rain rate distribution at NASA Rosman during ATS-5 data periods in 1970.

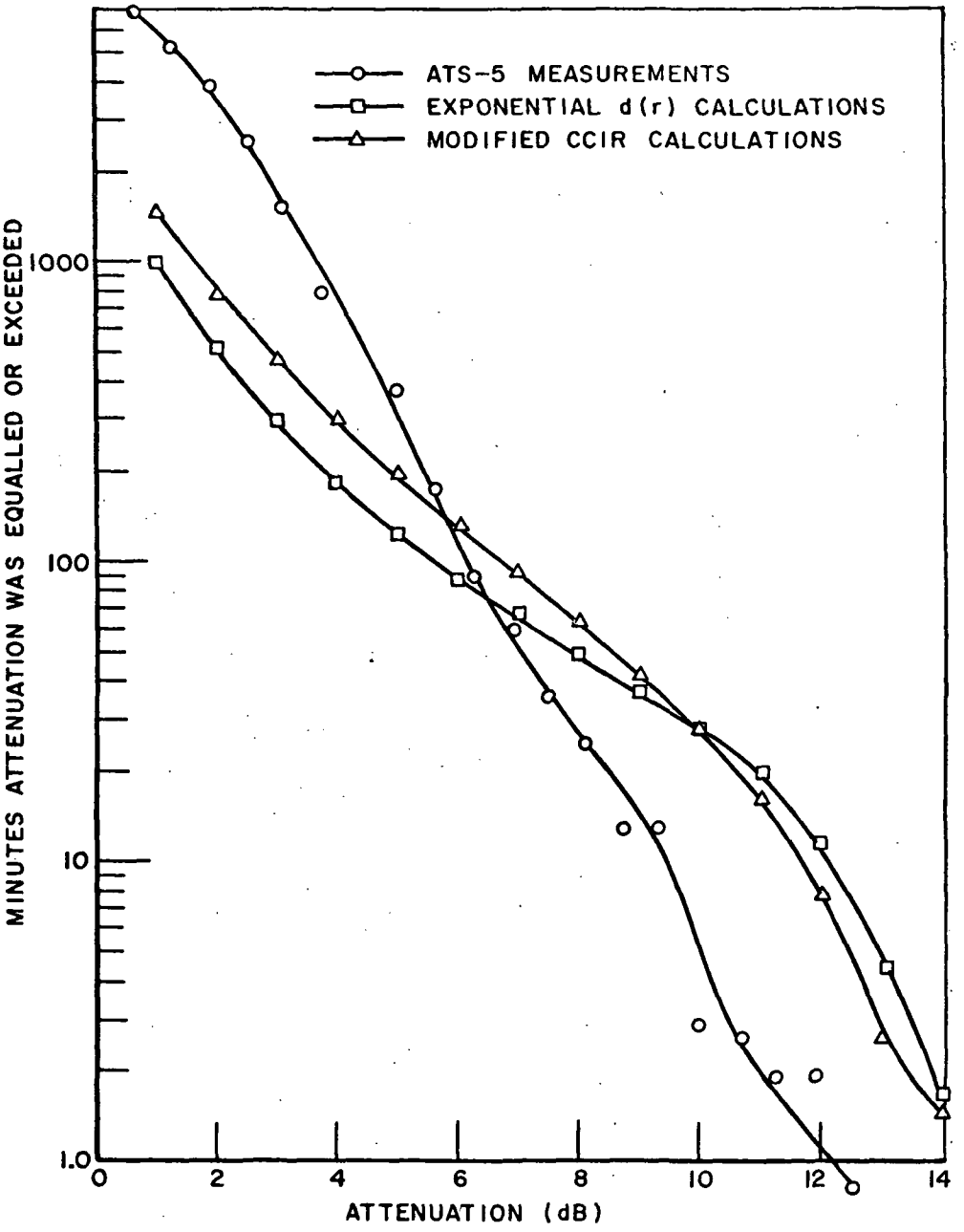

Fig. 18.--NASA ATS-5 1970 measured and calculated attenuation distribution.

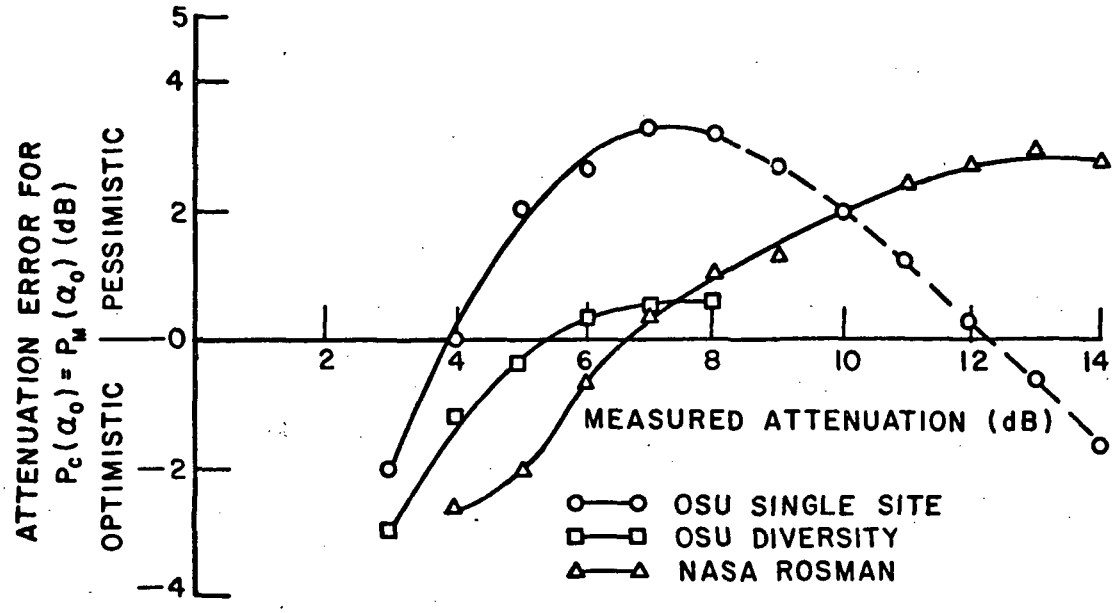

Fig. 19.--Comparison of calculated and measured 15.3 GHz ATS-5 1970 data using the exponential diameter function.

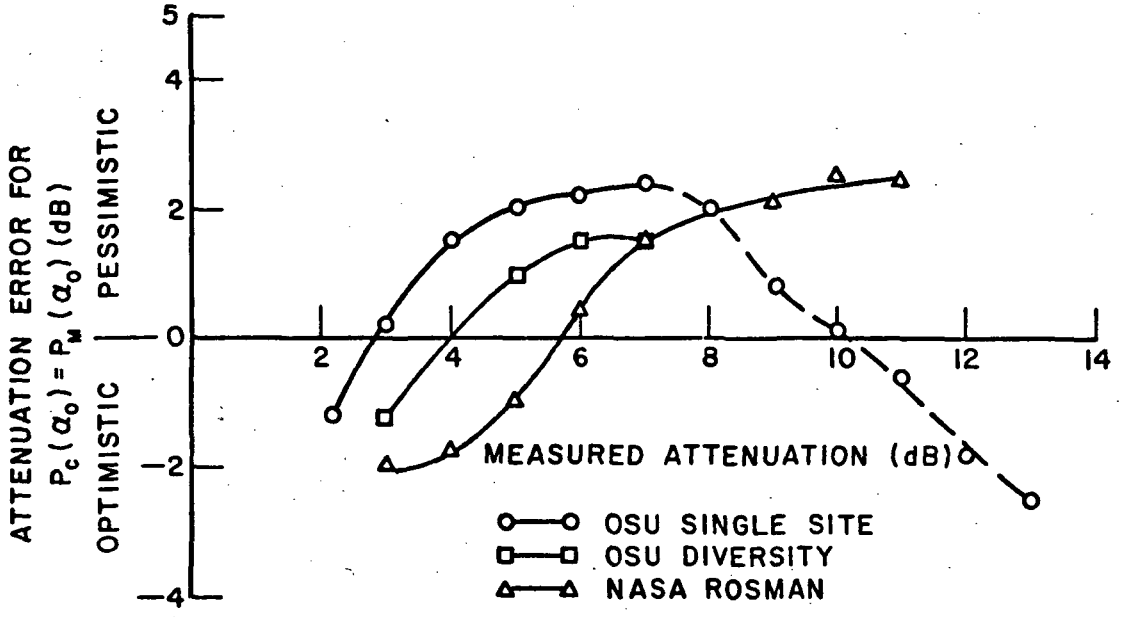

Fig. 20.--Comparison of calculated and measured 15.6 GHz ATS-5 1970 data using the modified CCIR diameter function.

millimeter wavelength attenuation statistics is potentially useful. The similarity of the error curves suggests that the present model has a systematic error that might be reduced by modifying the model parameters.

To examine the sensitivity of the model to variations of the model storm cell parameters a ten percent perturbation was imposed and the single site yearly attenuation probability distribution was calculated for the site located in Columbus, Ohio, using the Rice-Holmberg coefficients for the rain rate distribution function. It was found that there was little change in the calculated distribution due to elevation angle or the cell height changes. However, perturbations of the remaining parameters, d(r), k, and p had a significant effect on the probability distribution as shown in Figs. 21-25.

The parameter which showed the greatest sensitivity was p in Eq. (5), the Gunn-East attenuation relation. The ±10% perturbation caused the calculated value of $P(\alpha_0)$ to change more than 3 orders of magnitude for large attenuations. For a constant $P(\alpha_0)$, this corresponded to a ±5 dB change in α_0. The high sensitivity of the attenuation distribution to variations in p is probably due to several factors. First, p is an exponential constant greater than one, thus, the perturbations are exponentially magnified. Second, p influences both the lower limit of the r integration, $r_{min}(\alpha)$, and the minimum intersected path length, $\ell_1(\alpha_0,r)$.

The perturbations of the other constant in the Gunn-East relation, k, and the constants in the exponential cell diameter-rain rate function, d(r), were less severe. As seen in Figs. 22-25 the ±10% perturbation of the above named parameters resulted in an order

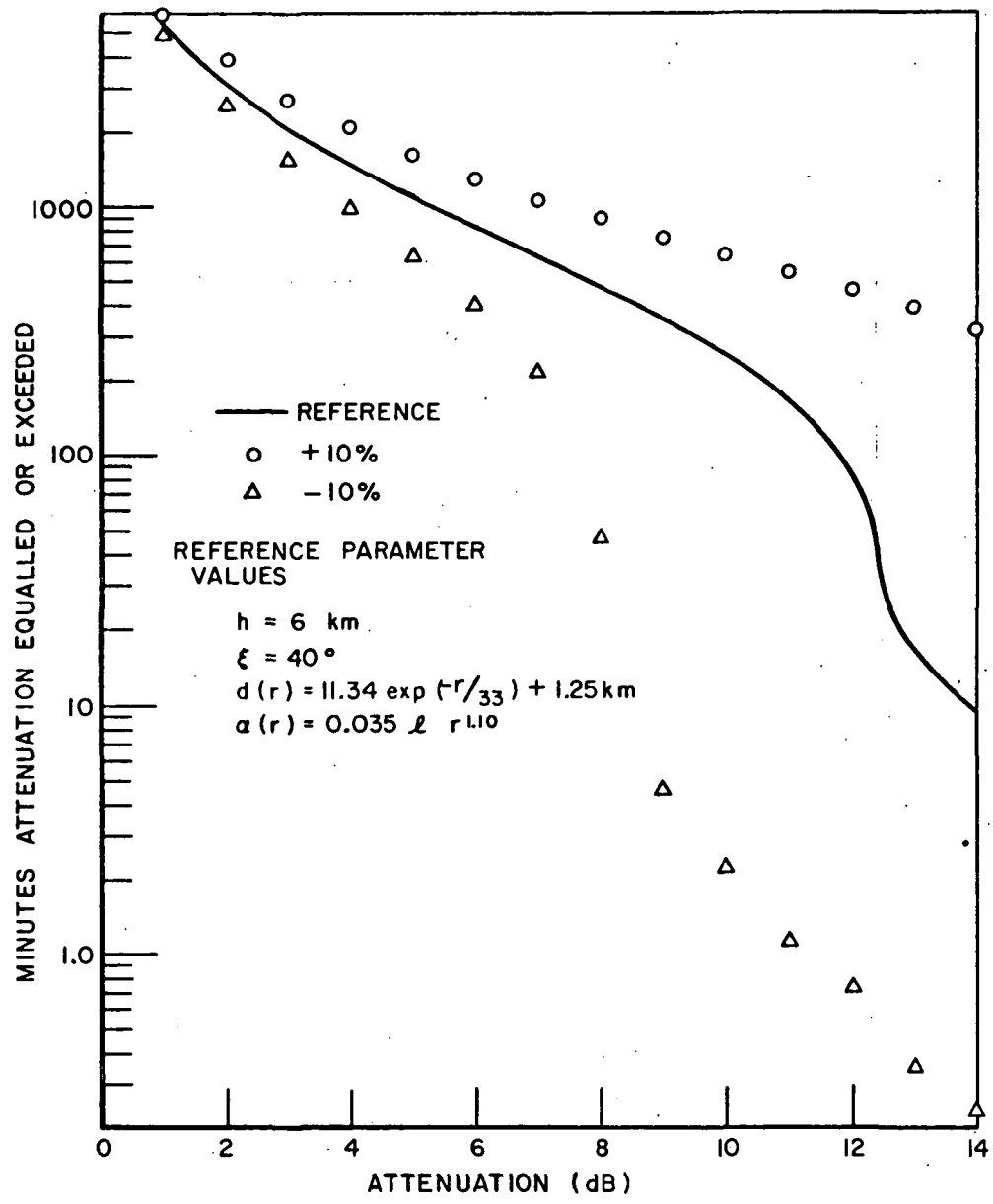

Fig. 21.--Effect of ±10 percent variation of the power, p, in $\alpha(R)$.

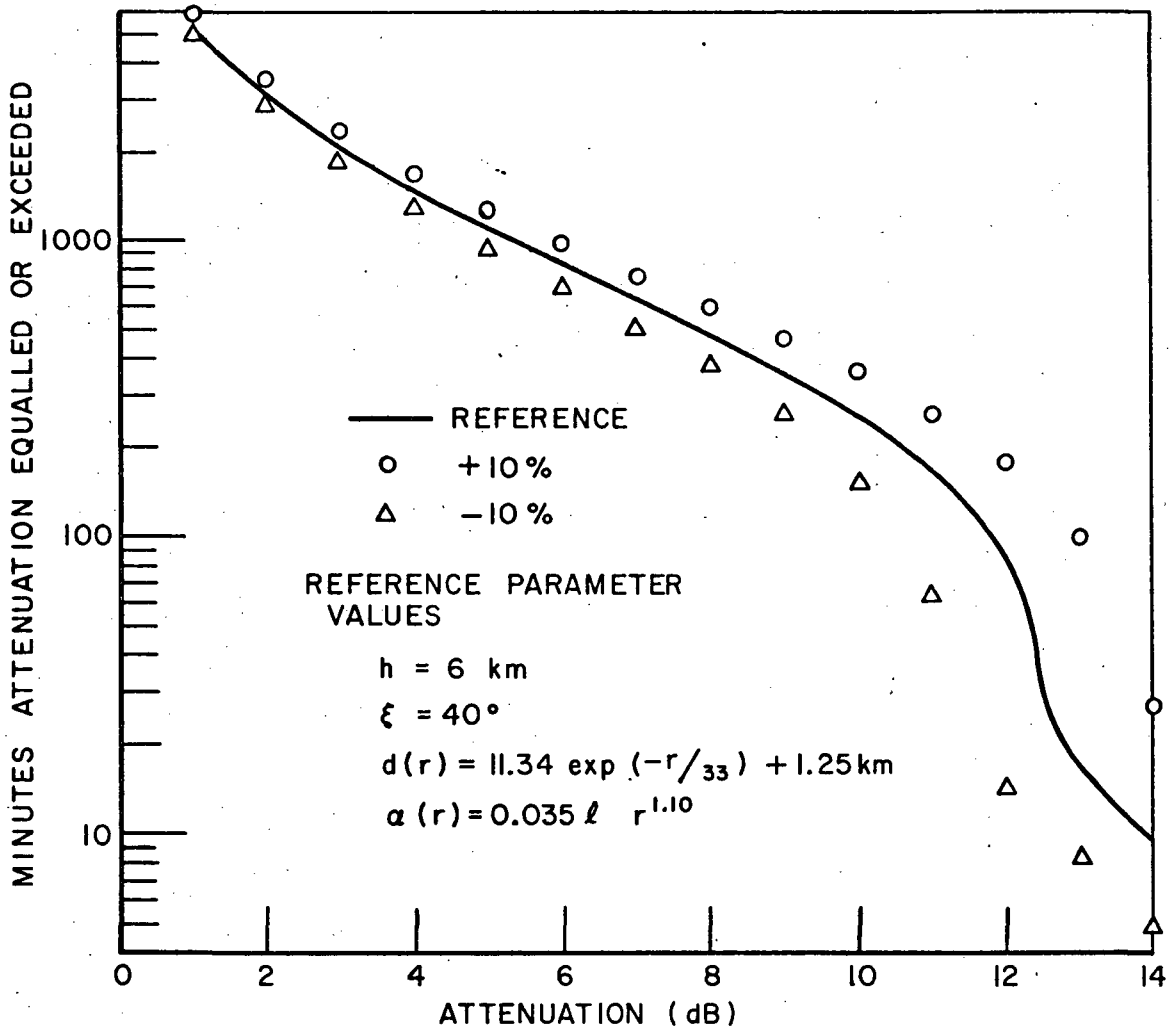

Fig. 22.--Effect of ±10 percent variation of the coefficient, k, in $\alpha(R)$.

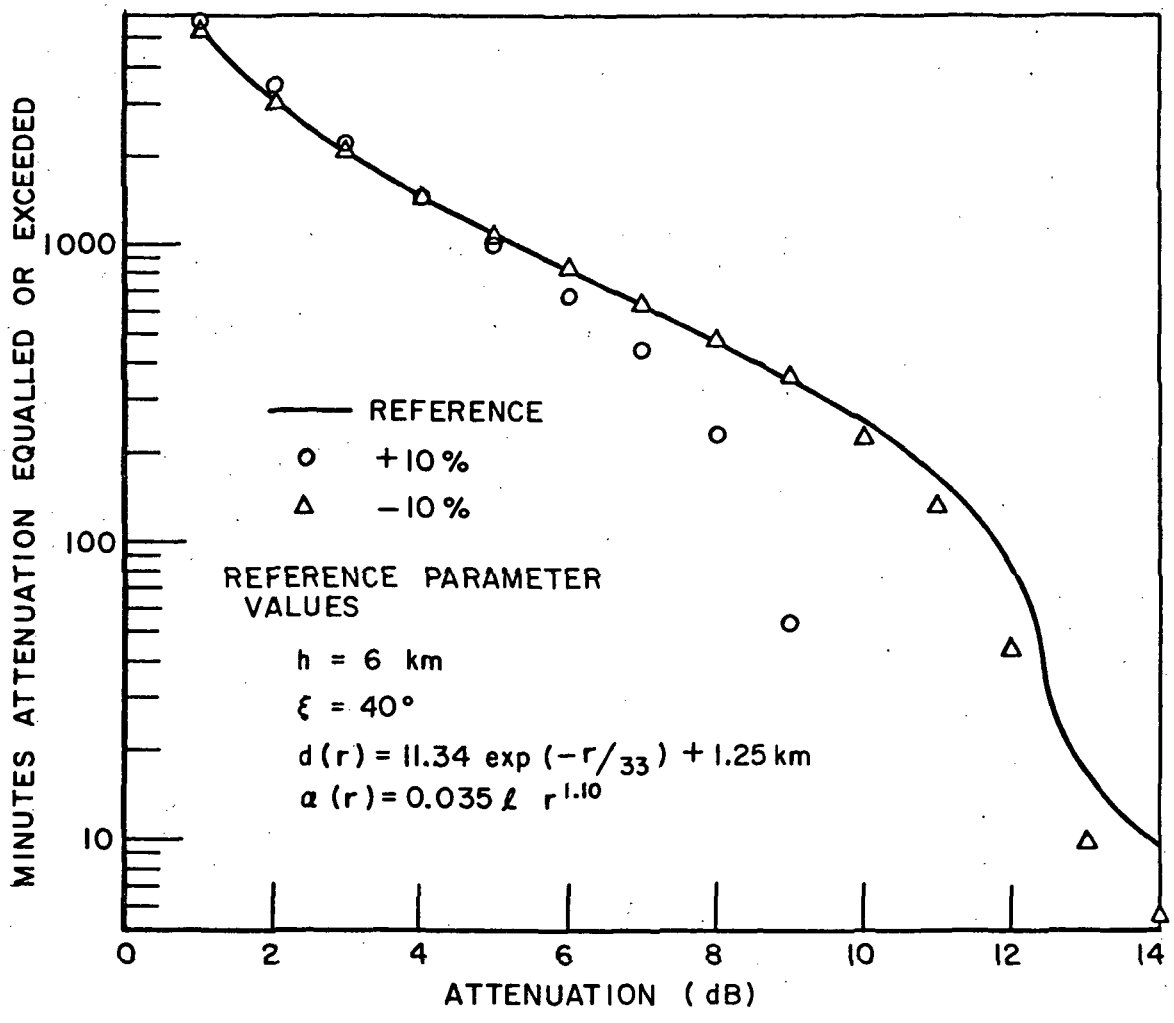

Fig. 23.--Effect of ±10 percent variation of the minimum cell diameter.

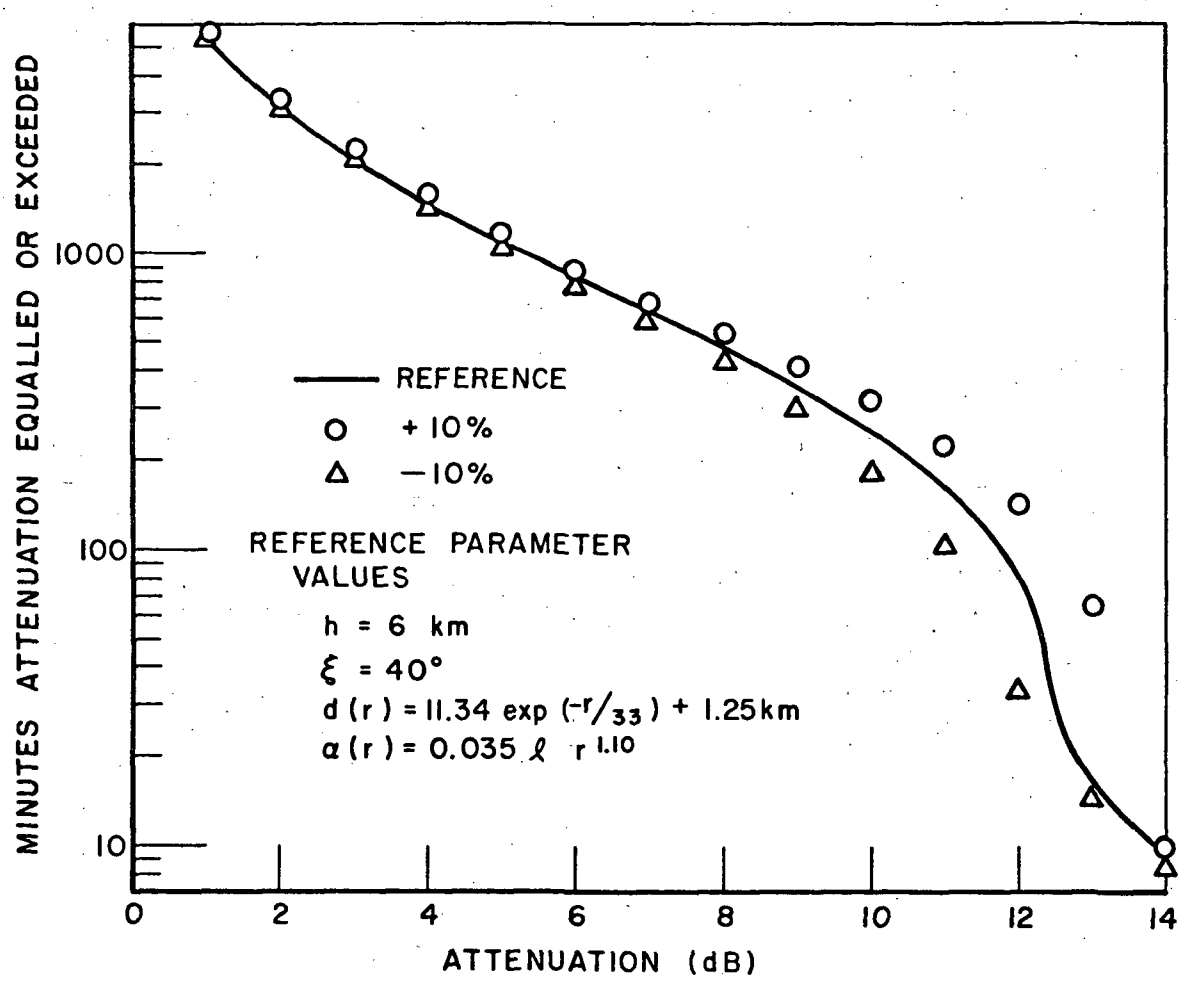

Fig. 24.--Effect of ±10 percent variation of cell diameter constant.

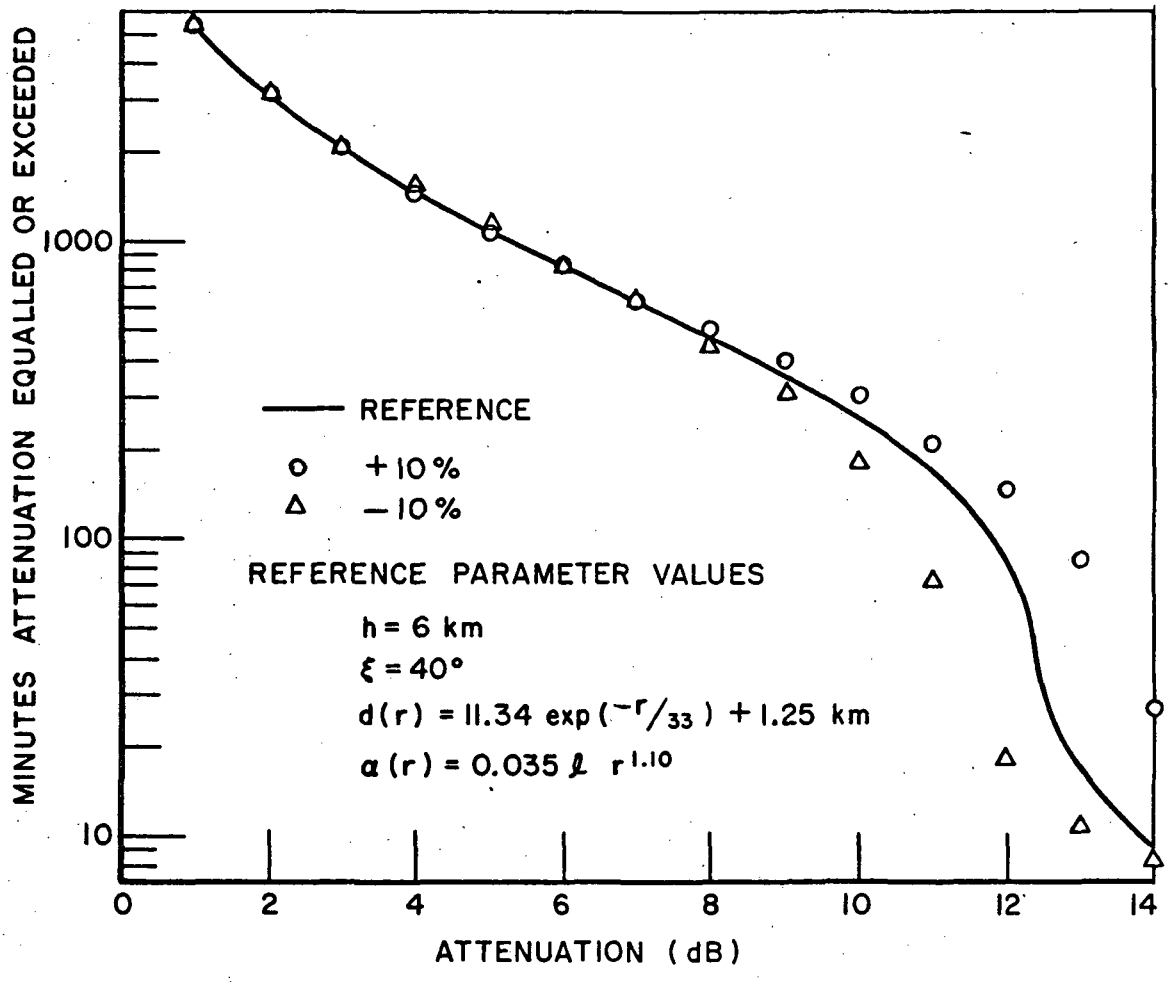

Fig. 25.--Effect of ±10 percent variation of cell diameter rate.

of magnitude variation in $P(\alpha_0)$ and at constant $P(\alpha_0)$, about a ±2 dB variation in α_0. Although these variations are significant, it is clear that the most critical constant is p in Eq. (5).

Ultimately the factor which will limit the accuracy of this model for use in terminal design is the yearly rainfall variation. To examine the magnitude of this variation, four years of rainfall data from the Port Columbus station of the National Weather Service were used to calculate the annual Rice-Holmberg clock-minute rain rate probability density functions. These coefficients were then used to calculate the attenuation probability distribution functions which are shown in Fig. 26. For reference the total yearly accumulations are also shown for each year. The largest variation of α_0 at a constant $P_\alpha(\alpha_0)$ is approximately ±1.5 dB. While this test does not necessarily represent a worst case it does provide a feeling for the order of magnitude of the variations that might be expected.

To improve the accuracy of the calculated attenuation probability function at the high attenuations, modifications to the model parameters were considered. The parameter which has the least certainty associated with its value is the diameter rain rate function and this function was examined. Following the idea presented by Rice and Holmberg, that three exponential modes were needed to approximate the rain rate distribution function, a three mode exponential function was postulated for the diameter rain rate function. Using the exponential diameter function as a starting point, the calculated attenuation probability distribution function for the Ohio State

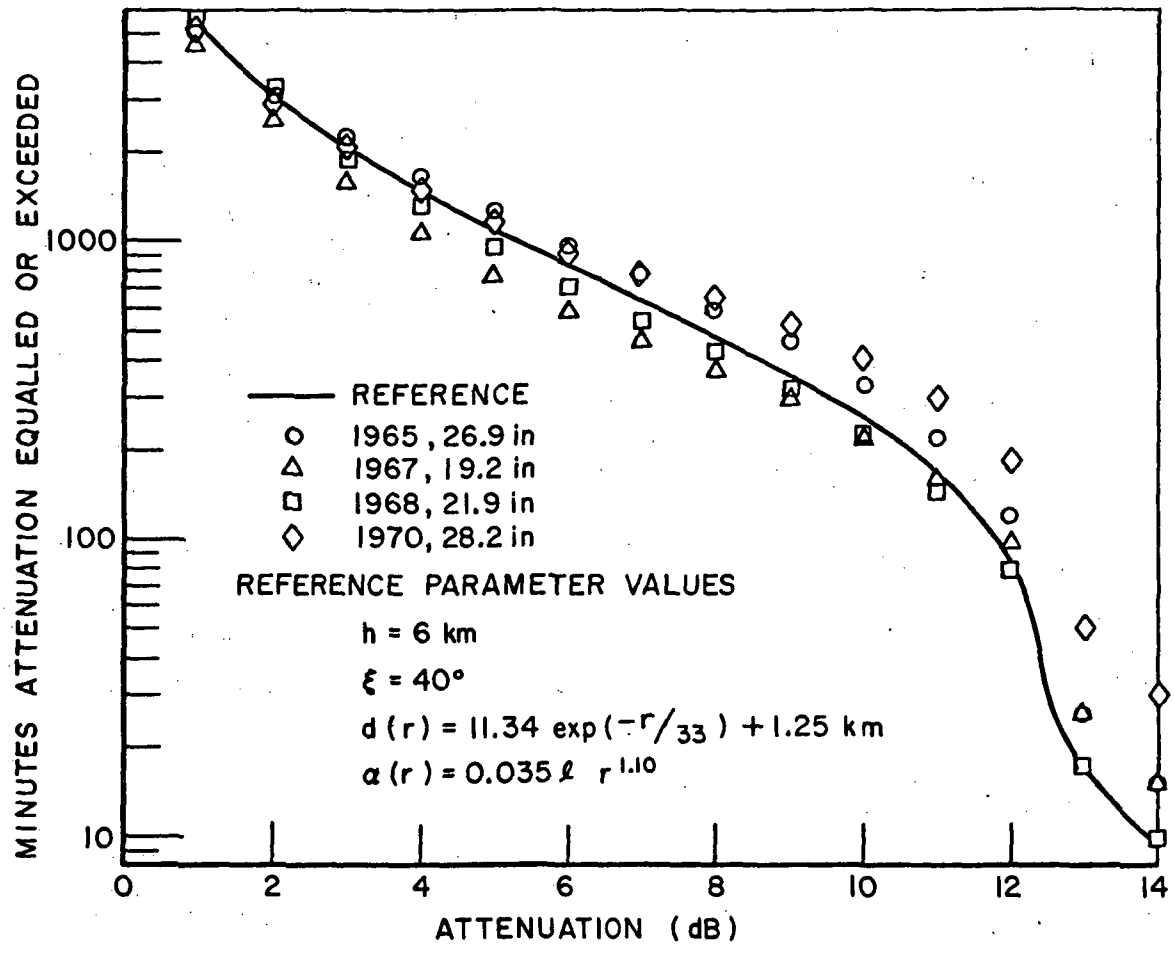

Fig. 26.--Effect of yearly weather variations for 1965, 1967, 1968 and 1970 at Columbus, Ohio.

University single terminal was fitted by trial-and-error to the measured data by modifying the diameter function parameters. The measurements above 8 dB attenuation were ignored since they were dominated by the system threshold. The resulting three mode diameter function is given in Eq. (65).

$$d(r) = 1134.\ \exp(-r/3.5) + 1.13\ \exp(-r/33) + 1.25\ \exp(-r/264)\ \text{(km)}. \tag{65}$$

For comparison the diameter function in Eq. (65) is shown in Fig. 27

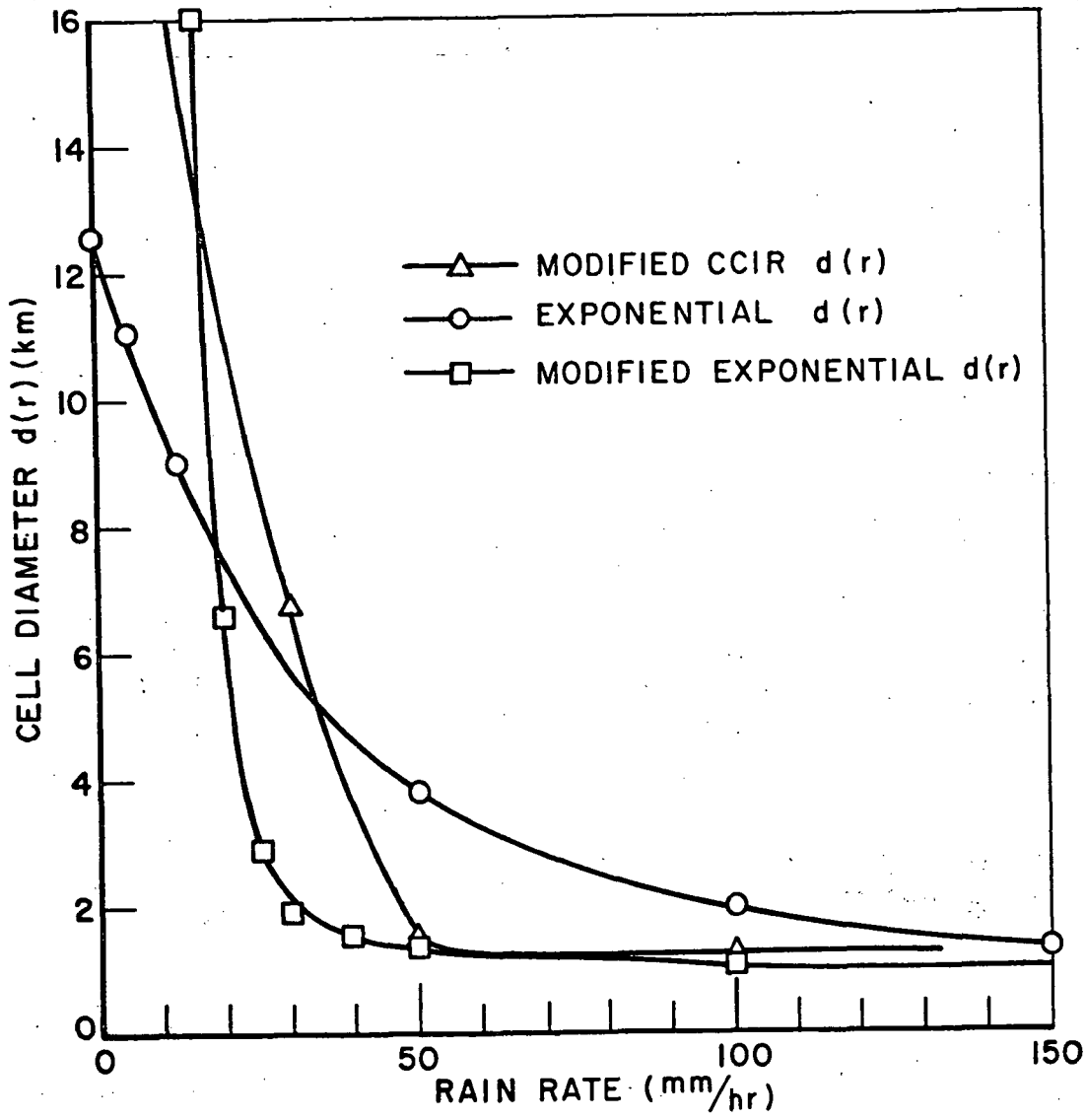

Fig. 27.--Comparison of three rain rate diameter relationships.

with the diameter functions mentioned earlier. It is seen that the three mode diameter function is similar to the CCIR relation with two exceptions. First, Eq. (65) is approaching a finite but large value at r=0. Second, Eq. (65) decays exponentially for high rain rates.

The resulting attenuation probability distributions are shown in Fig. 28. It is seen that the general shape of the single terminal

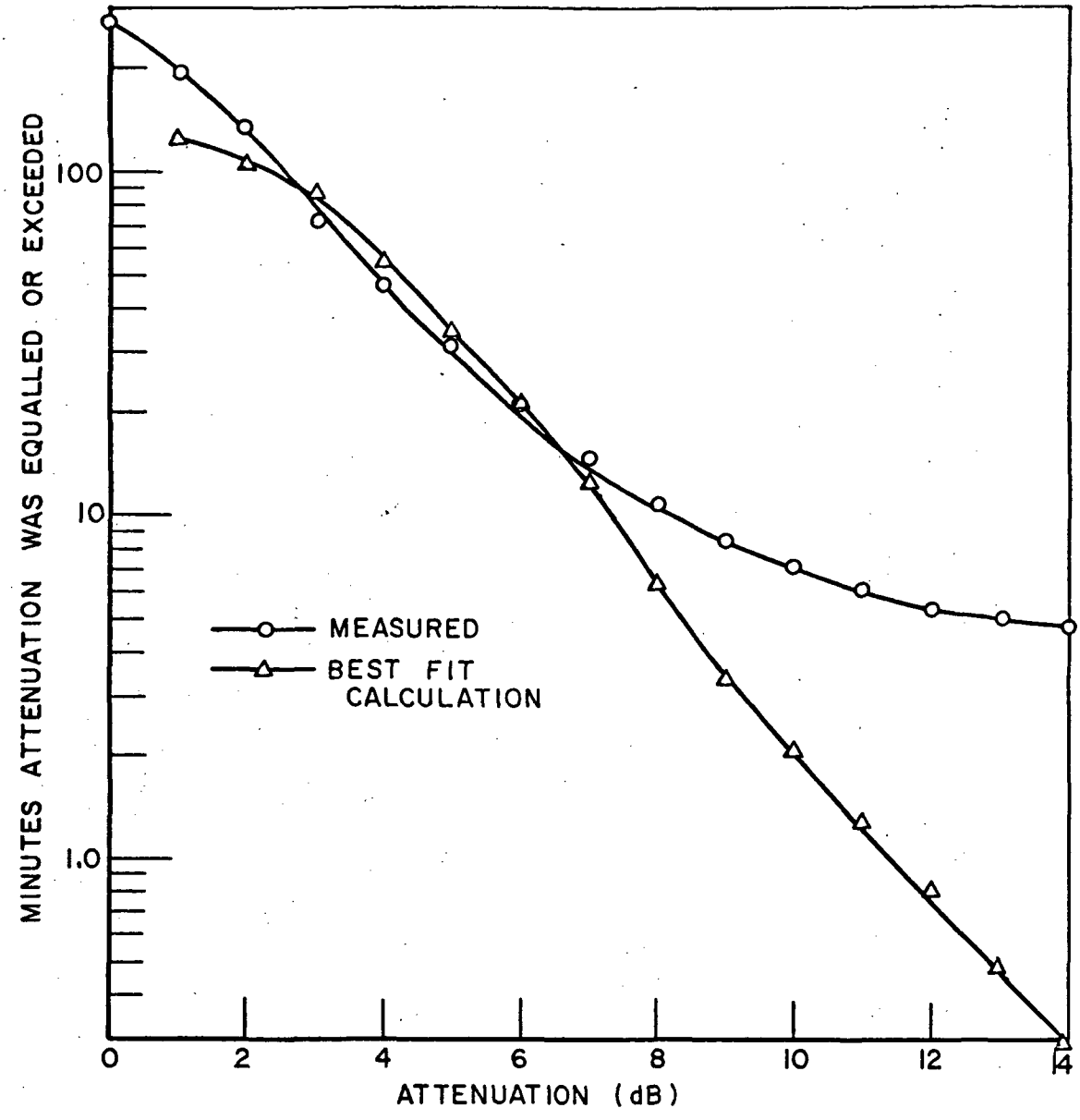

Fig. 28.--Ohio State University ATS-5 single site measured and calculated joint distribution for modified diameter function.

probability distribution has been approximated if the threshold flattening of the experimental data for large attenuations is ignored.

Using this new diameter function the diversity attenuation distribution was calculated and is shown with the measured distribution in Fig. 29. It is seen that good agreement has also been

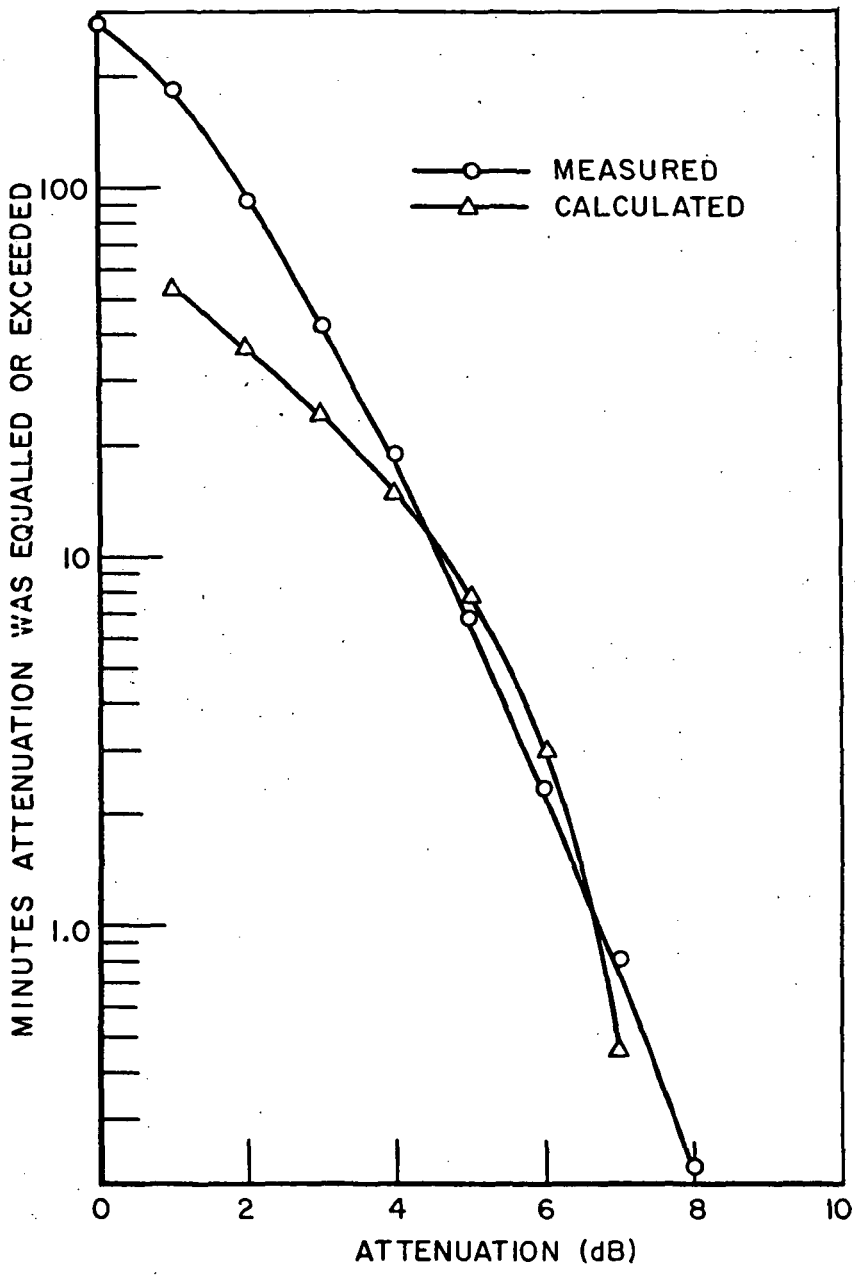

Fig. 29.--Ohio State University ATS-5 diversity site measured and calculated joint distribution for modified diameter function.

obtained here. As a further test of the new diameter function, the attenuation distribution was calculated for the NASA terminal and the results shown in Fig. 30. The agreement between the calculated

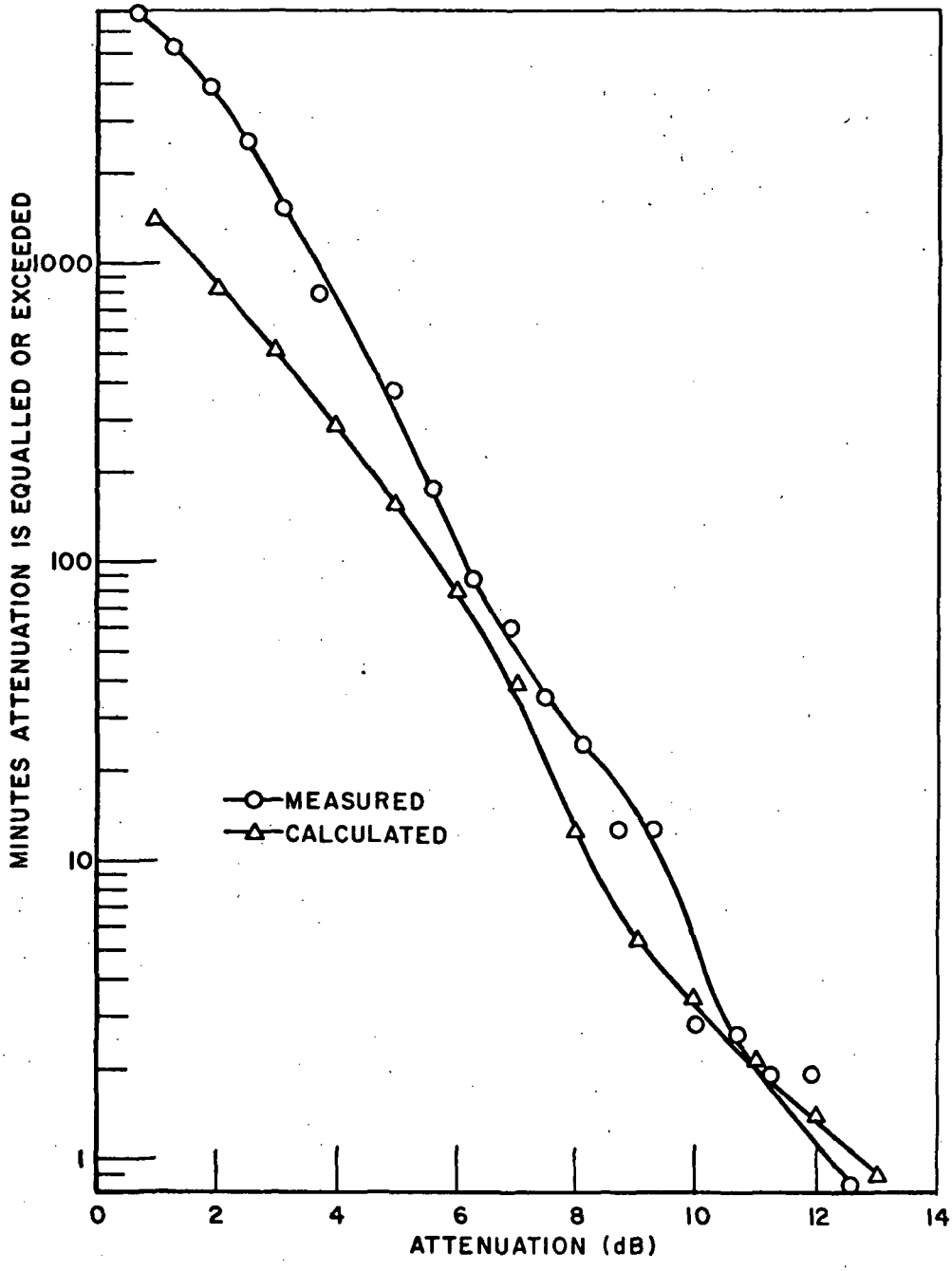

Fig. 30.--NASA ATS-5 measured and calculated attenuation distribution for modified diameter function.

and experimental distributions has been improved here also. The errors are summarized by the error curves in Fig. 31. It is seen that

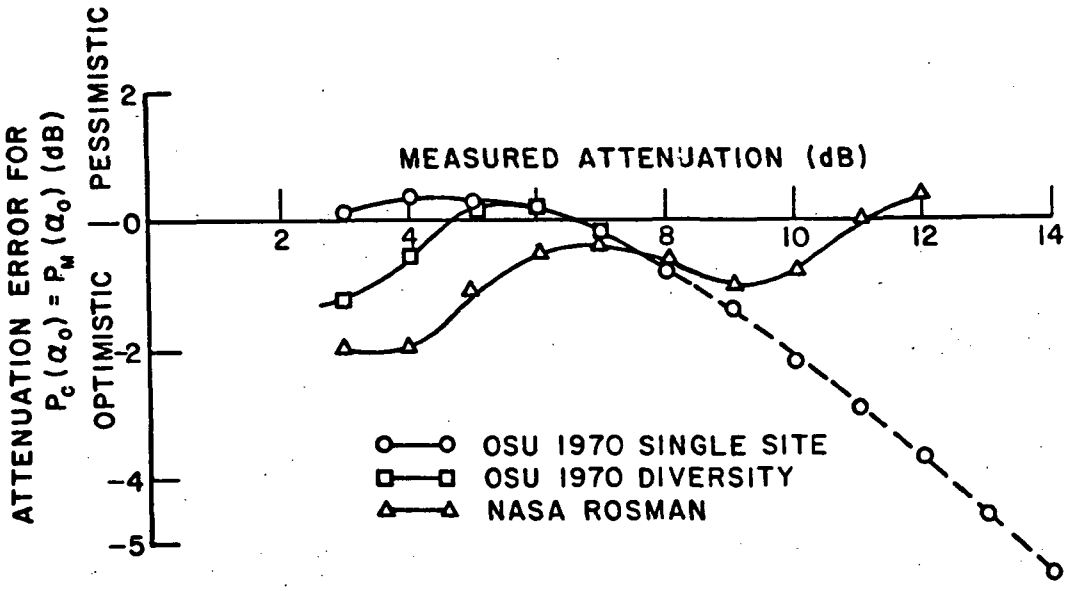

Fig. 31.--Attenuation error for three mode diameter function.

using the three mode diameter function the range of the error in predicting the attenuation is between +1 and -2 dB. Therefore, millimeter wavelength attenuation distributions for single terminal and two terminal diversity configurations can be calculated with reasonable accuracy using this simple storm cell model.

CHAPTER VI
SUMMARY

In conclusion, a cylindrical, single storm cell model was postulated. The attenuation probability distribution for an earth-space propagation path was calculated for both a single earth terminal and a spatial diversity terminal configuration. The calculation procedure used a tipping bucket rain rate distribution function, a storm cell diameter-rain rate function, a fixed cell height and the Gunn-East attenuation-rain rate relation as parameters. The tipping bucket rain rate distribution function proposed by Rice and Holmberg was discussed and its usefulness is making calculations for a particular geographic location from tipping bucket rain rate measurements was discussed. A cell diameter-rain rate function measured by Hogg and a diameter function proposed by CCIR were presented. Also discussed were typical values for the model storm cell height.

The attenuation distribution functions for two ATS-5 Millimeter Wavelength Experiment receiving stations were calculated using the chosen cell parameters and measured tipping bucket rain rate data. The calculated distributions agreed within 3 dB of the measured distributions. The sensitivity of the calculated results to parameter variations was discussed and it was determined that the rain rate exponent in the Gunn-East relation was the most critical parameter, causing a 5 dB variation in the prediction for a 10% variation.

It was also found that yearly precipitation variations could cause at least a 1.5 dB variation in the attenuation distribution.

To improve the accuracy of the calculated attenuation distribution, a three mode exponential diameter function was postulated and the Ohio State University single site measured attenuation probability distribution was used to determine the diameter function coefficients. The three mode diameter function was then used to calculate the Ohio State University diversity attenuation distribution and the NASA Rosman single site attenuation distribution. The calculated distributions agreed within -2 to +1 dB of the measured distributions which represented a significant improvement over the other diameter functions used.

Thus, it has been shown that a simple cylindrical storm cell model is useful in predicting millimeter wavelength precipitation attenuation. The model proposed is mathematically tractable and sufficiently general so that modification can be easily made.

REFERENCES

1. Moore, L., "A Guide to Commercial and Military Satellite Systems: Part 1," Microwave System News, 2, No. 8, 1971, pp. 10-14.
2. "The DOMSAT Derby," Microwave System News, 2, No. 8, 1971, pp. 3-7.
3. Ippolito, L.J., "Effects of Precipitation on 15.3 and 31.65 GHz Earth-Space Transmissions with ATS-5 Satellite," Proc. of IEEE, 59, 1971, pp. 189-205.
4. Dutton, E.J., "Estimation of Radio Ray Attenuation in Convective Rainfalls," J. Applied Meteorology, 6, 1967, pp. 662-668.
5. Bradley, I.H.S., "Rainfall Extreme Value Statistics Applied to Microwave Attenuation Climatology," McGill Stormy Weather Group Scientific Report MU-66, McGill University, 1970.
6. Bussey, H.E., "Microwave Attenuation Estimated From Rainfall and Water Vapor Statistics," Proc. IRE, 38, p. 781.
7. Gunn, K.L.S. and East, T.W.L., "The Microwave Properties of Precipitation Particles," Quarterly Journal of the Royal Meteorological Society, 80, No. 346, 1954, pp. 522-545.

8. Papoulis, A., Probability, Random Variables, and Stochastic Processes, McGraw Hill, New York, N.Y., 1965.

9. Hourly Precipitation Data, U.S. Department of Commerce, Environmental Data Service, Asheville, North Carolina.

10. Bussey, H.E., "Microwave Attenuation Statistics Estimated from Rainfall and Water Vapor Statistics," Proc. IRE, 38, 1950, pp. 781-785.

11. Cole, A.E., Donaldson, R.J., Dyer, R., Kantor, A.J., and Skrivanek, R.A., "Precipitation and Clouds: A Revision of Chapter 5, Handbook of Geophysics and Space Environments," Air Force Surveys in Geophysics, No. 212, Air Force Cambridge Research Laboratories, 1969.

12. Dyck, H.D. and Mattice, W.A., "A Study of Excessive Rainfall," Monthly Weather Review, 69, 1941, p. 293.

13. Lenhard, R.W., Cole, A.E. and Sissenwine, N., "Preliminary Models for Determining Instantaneous Precipitation Intensities From Available Climatology," Environmental Research Papers, No. 350, Air Force Cambridge Research Laboratories.

14. Rice, P.L. and Holmberg, N.R., Private Communication, ITS Laboratory, Boulder, Colorado.

15. Hogg, D.C., "Rain on Earth-Space Paths," 1971 G-AP International Fall Symposium, Los Angeles, California.

16. Benoit, A., "Signal Attenuation Due to Neutral Oxygen and Water Vapor, Rain and Clouds," The Microwave Journal, November, 1968, p. 73.

17. Byers, H., The Thunderstorm, Report of The Thunderstorm Project, Department of Commerce, Washington D.C., 1949.

18. Crane, R.K., "Coordination Area For Mainlobe-to-Mainlobe Coupling Due to Rain Scatter," 1971 G-AP International Fall Symposium, Los Angeles, California.

19. Medhurst, R.G., "Rainfall Attenuation of Centimeter Waves: Comparison of Theory and Measurement," IEEE Trans. Antennas and Propagation, AP-13, 1965, pp. 550-564.

20. Crane, R.K., "Propagation Phenomenon Affecting Satellite Communications Systems Operating in the Centimeter and Millimeter Wavelength Bands," Proc. IEEE, 59, 1971, pp. 173-189.

21. Ippolito, L.J., "Millimeter Wave Propagation Measurements from Applications Technology Satellite (ATS-5)," IEEE Trans. Antennas and Propagation, AP-8, 1970, p. 335.

22. Semiannual Status Report, "Millimeter-Wavelengths Propagation Studies," Report 2374-3, 15 April 1969, ElectroScience Laboratory, Department of Electrical Engineering, The Ohio State University; prepared under Grant No. NGR-36-008-080 for National Aeronautics and Space Administration.

23. Semiannual Status Report, "Millimeter-Wavelengths Propagation Studies," Report 2374-4, 30 April 1970, ElectroScience Laboratory, Department of Electrical Engineering, The Ohio State University; prepared under Grant No. NGR-36-008-080 for National Aeronautics and Space Administration.

24. Grimm, K.R. and Hodge, D.B., "A 15.3 GHz Satellite-To-Ground Diversity Propagation Experiment Using a Terminal Separation of 4 Kilometers," Report 2374-7, December 1971, ElectroScience Laboratory, Department of Electrical Engineering, The Ohio State University; prepared under Grant No. NGR-36-008-080 for National Aeronautics and Space Administration.

25. Harman, L., Private Communication, Westinghouse Electric Corporation.

26. Mondre, E., "Atmospheric Effects on Millimeter Wave Communication Channels," NASA Document X-733-70-250, March 1970, p. 15.